Electronic nonadiabatic effects in low temperature radical-radical reactions. I. C(3P) + OH(2)

A. I. Maergoiz, E. E. Nikitin, and J. Troe

Citation: The Journal of Chemical Physics **141**, 044302 (2014); doi: 10.1063/1.4889996
View online: http://dx.doi.org/10.1063/1.4889996
View Table of Contents: http://scitation.aip.org/content/aip/journal/jcp/141/4?ver=pdfcov
Published by the AIP Publishing

Electronic nonadiabatic effects in low temperature radical-radical reactions. I. C(^{3}P) + OH($^2\Pi$)

A. I. Maergoiz,[1] E. E. Nikitin,[2,3] and J. Troe[1,2,a)]
[1]*Institut für Physikalische Chemie, Universität Göttingen, Tammannstrasse 6, Göttingen D-37077, Germany*
[2]*Max-Planck-Institut für Biophysikalische Chemie, Am Fassberg 11, Göttingen D-37077, Germany*
[3]*Schulich Faculty of Chemistry, Technion – Israel Institute of Technology, Haifa 32000, Israel*

(Received 25 February 2014; accepted 30 June 2014; published online 23 July 2014)

The formation of collision complexes, as a first step towards reaction, in collisions between two open-electronic shell radicals is treated within an adiabatic channel approach. Adiabatic channel potentials are constructed on the basis of asymptotic electrostatic, induction, dispersion, and exchange interactions, accounting for spin-orbit coupling within the multitude of electronic states arising from the separated reactants. Suitable coupling schemes (such as rotational + electronic) are designed to secure maximum adiabaticity of the channels. The reaction between C(^{3}P) and OH($^2\Pi$) is treated as a representative example. The results show that the low temperature association rate coefficients in general cannot be represented by results obtained with a single (generally the lowest) potential energy surface of the adduct, asymptotically reaching the lowest fine-structure states of the reactants, and a factor accounting for the thermal population of the latter states. Instead, the influence of non-Born–Oppenheimer couplings within the multitude of electronic states arising during the encounter markedly increases the capture rates. This effect extends up to temperatures of several hundred K.
 [http://dx.doi.org/10.1063/1.4889996]

I. INTRODUCTION

Radical-radical reactions at low temperature present a particular challenge to rate theory. Open-electronic shell radicals in electronically degenerate or nearly-degenerate states approach each other in a multitude of bonding or repulsive electronic states which generally will interact in the course of the formation of reaction adducts. While quantum scattering or classical trajectory (CT) calculations on single Born-Oppenheimer (SBO) potential energy surfaces (PESs) can be done today with remarkable precision (see, e.g., Ref. 1), the influence of the multitude of interacting electronic potentials so far has only rarely been taken into account in a satisfactory manner. Mostly, SBO rate constants for adduct formation on the lowest PES, $k_{\rm cap}^{\rm SBO}$, have been multiplied by a factor $f_{\rm el}(T)$ accounting for the thermal population of the lowest electronic fine-structure levels of the separated radicals, see, e.g., Refs. 2–5. The Born–Oppenheimer (BO) approximation of an adiabatic correlation between the reactant and adduct ground (X) electronic states, which is implicitly followed in this approach, then leads to the corresponding capture rate constant

$$k_{\rm cap}^{\rm X,\,BO} \approx f_{\rm el}(T) k_{\rm cap}^{\rm SBO}. \qquad (1.1)$$

It is the aim of the present work to show that the described procedure – at least for low temperature conditions – will generally not be adequate. However, a full quantum scattering calculation including all electronic states at present still appears at the limit of feasibility. We, therefore, propose an alternative simpler approach which has been successful for SBO processes under high temperature conditions. We design adiabatic channels whose quantum numbers are (nearly) conserved during the course of adduct formation and which show a minimum of nonadiabaticity generated by the kinetic energy of the approaching radicals. In the original version of the adiabatic channel (AC) model (the statistical AC model, SACM, of Ref. 6), adiabatic channel potentials $V_i(R)$ were obtained as eigenvalues of the Hamiltonian at fixed interreactant center-of-mass distances R neglecting the orbital rotation. Adding orbital energy, each channel with the quantum number i has its specific centrifugal energy barrier $E_{0,\,i}(\ell)$, and these barriers with increasing orbital quantum number ℓ often move towards smaller R, an effect which can be mimicked by variational transition state theory (although the results are not the same[6]). The task of diagonalizing the Hamiltonian at each R was simplified by separating conserved and transitional modes, by correlating states of the latter modes for separated and combined reactants, and by further simplifying the calculation of the $V_i(R)$ by the use of exponential switching models. Nonadiabatic transitions between adiabatic channels, induced by the motion along R and related to crossings and avoided crossings of the $V_i(R)$, were accounted for in different ways, see, e.g., the post-adiabatic channel approach of Ref. 7. Alternatively, either the dynamics of the transitional modes was treated by classical trajectories (CT) and combined with adiabatic dynamics of the conserved modes (the AC-CT concept of Refs. 8–12), or Coriolis coupling was treated in an axially nonadiabatic channel approach.[13] For high temperature applications, SBO-AC and AC-CT treatments were shown to lead to the same results.[14] On the other hand, quantum models are required for ultralow temperature applications.[15–18] One should note that the AC concept can

a)Electronic mail: shoff@gwdg.de.

be exploited in a variety of ways. Besides capture rate constants also capture cross sections in scattering theory have been expressed in terms of numbers of open ACs, see, e.g., Refs. 2 and 19–21. Likewise, lifetimes of dissociating species may be expressed with numbers of open ACs.[22,23] Although the details of numerically characterizing ACs may differ in the various approaches, the general equivalence of the concept has been elaborated and emphasized, see, e.g., Refs. 24 and 25.

After having formed an adduct by capture, this adduct may redissociate or move on to form new species. Capture and redissociation obviously are related by microscopic reversibility while the formation of new species involves different ACs. Provided that the internal dynamics is sufficiently strongly coupled and leads to randomization, the overall rate constant may be expressed fully statistically in terms of numbers of open "entrance" and "exit" ACs. Alternatively, partially statistical or completely nonstatistical behavior of the adduct may be observed, while the entrance and exit dynamics still be adequately described by the corresponding ACs. Whatever the type of reaction, ACs have a far reaching relevance[20] and the present work, by extending SACM beyond the SBO results of Refs. 6 and 8–12, provides AC potentials for general applications.

When two open-electronic shell species approach each other, a multitude of Born-Oppenheimer (MBO) electronic states is generated. One may be tempted to formulate ACs for these states individually such as described before,[6] and assume electronically adiabatic behavior. For example, one may postulate that the dynamics of the system that starts on the lowest electronic state of the separated reactants will bring the system to the lowest BO state of the adduct. A consequence of this assumption is the concept of Eq. (1.1), i.e., of a weighting of the SBO results by the thermal population of specific electronic states at the entrance of the reaction. Whenever non-BO couplings between the MBO electronic states are present and the coupling between various electronic states of the separated reactants upon approach gains importance, this treatment becomes questionable. This is the problem which is addressed in the following article. Adiabatic channels now are constructed in a way different from SBO situations and being specific for each radical-radical reaction. Adiabatic channel potentials are defined within a non-Born-Oppenheimer (NBO) approach. We take the capture of $C(^3P)$ by $OH(^2\Pi)$ as a representative example. We have chosen this system for a number of reasons. First, there have been high-level SBO calculations for this system which, with the help of Eq. (1.1), led to low temperature rate constants[26–31] such as considered also in the present work. This allows us to compare the present results with this alternative treatment and to inspect the validity (or non-validity) of an approach based on Eq. (1.1). Furthermore, long-range asymptotic potentials for the 18 doubly degenerate MBO states arising from $C(^3P) + OH(^2\Pi)$, such as characterized in Ref. 28, are complemented in our work by the contributions from the asymptotic electronic exchange interaction which, at intermediate interreactant distances, results in a separation of the electronic states of the adduct which finally can be characterized by total spin and reflection symmetry (the total electronic moment is averaged to zero). In this way capture into various electronic states of the adduct can also be differentiated.

Other treatments of triatomic radical-radical reactions so far essentially were limited to SBO approaches employing Eq. (1.1). For instance, the reaction $O + OH \leftrightarrow HO_2 \leftrightarrow H + O_2$ was treated in Refs. 1, 14, and 32–39, $O + O_2 \leftrightarrow O_3$ in Refs. 40–42, $S + OH \leftrightarrow HSO \leftrightarrow H + SO$ in Refs. 38 and 43, $N + OH \leftrightarrow HNO \leftrightarrow H + NO$ in Refs. 38 and 44–46, and $Si + OH \leftrightarrow HSiO \leftrightarrow H + SiO$ in Ref. 47. A preliminary treatment of the reaction $O(^3P) + OH(^2\Pi)$ within our asymptotic adiabatic channel approach was presented in Ref. 32. However, this work needs a continuation with the goal to resolve the discrepancies between the various experimental and theoretical results, see Ref. 1.

The plan of the present article is the following. Section II describes Hamiltonian, basis functions and potential energy surfaces of our asymptotic approach. Section III is devoted to the determination of AC potential curves for the C + OH reaction, with and without artificially switching off spin-orbit coupling. Section IV describes the implementation of the AC potentials into SACM expressions for thermal rate coefficients of capture into various electronic states of the adduct. It also discusses the differences between SBO calculations as corrected by Eq. (1.1) and NBOAC calculations. Finally, Section V concludes the article.

II. ASYMPTOTIC HAMILTONIAN AND POTENTIAL ENERGY SURFACES

A. Hamiltonians, quantum numbers, and basis functions

Following the general concept of SACM,[6,20] the Hamiltonian $\hat{H}$ of the system is formulated and its eigenvalues, the adiabatic channel potential curves $V_i(R)$, are calculated for fixed interreactant center-of-mass distance R. For situations where a SBO treatment suffices, $\hat{H}$ is expressed by the sum of the electronic state potential E_{el}, the orbital energy of the nuclear framework $T_{nuc}^{rot}(R)$, and the Hamiltonian $\hat{H}_{int}$ of the remaining coordinates which may (or may not) be separated into contributions from "conserved" and "transitional" modes. In the present MBO treatment with strong NBO couplings, a separation between the multitude of electronic potentials and the Hamiltonian $\hat{H}_{int}$ cannot be made. Instead, effective adiabatic channel potentials curves $V_i(R)$ are defined as sums of eigenvalues of the rotronic (rotational and electronic) Hamiltonian $\hat{H}^{rotr}$ and the orbital energy $T_{nuc}^{rot}(R)$, i.e., one employs a Hamiltonian

$$\hat{H} = \hat{H}^{rotr} + T_{nuc}^{rot}(R). \tag{2.1}$$

Here $\hat{H}^{rotr}$ is referred to the interreactant axis **R** which is assumed stationary in space. In the present calculations, for C + OH with fast rotating OH, the Coriolis interaction arising from the gyroscopic properties of the rotronic motion in the reference frame of the rotating interreactant axis **R**, is neglected. We assume that adiabatic channels constructed in the described way show the largest degree of adiabaticity in the association dynamics. We emphasize, however, that this assumption needs to be validated by calculations of

nonadiabatic effects induced by the relative motion or, finally, by full quantum scattering calculations, see above.

In the present work, following Ref. 32, we express the Hamiltonian $\hat{H}^{\rm rotr}$ by asymptotic theory, i.e., we employ its long-range limiting form. In the special case of C + OH capture considered here, the rotronic Hamiltonian $\hat{H}^{\rm rotr}$ includes the long-range interaction $U^{\rm lr}$ between the C atom and the OH molecule (represented by multipole electrostatic, dispersion, and induction terms), the asymptotic exchange interaction $U^{\rm ex}$ between the outer valence and uppermost inner electronic shells of C and OH, the Russel-Saunders spin-orbit coupling $\hat{H}_{\rm C}^{\rm SO}$ of the free C(^3P) atom, and the Hamiltonian $\hat{H}_{\rm OH}^{\rm rotr}$ of the rotating OH molecule in an approximation sufficient to describe the manifold of the rotronic states of isolated OH($^2\Pi$). It is essential that our asymptotic Hamiltonian includes the exchange interaction $U^{\rm ex}$. Without this contribution the derived AC potential curves $V_i(R)$ at short distance could not be attributed to their respective BO states of the adduct. One should note that the Hamiltonian $\hat{H}_{\rm OH}^{\rm rotr}$ of OH corresponds to a situation intermediate between Hund's coupling cases *a* and *b* (for the matrix representation in Hund's coupling cases *a* and *b*, see, e.g., Ref. 48). Λ- or Ω-doubling effects in the free reactant OH are ignored. One should furthermore take into account that, in contrast to $U^{\rm lr}$ and $U^{\rm ex}$, the part

$$\hat{H}_{\rm C,OH}^{\rm rotr} = \hat{H}_{\rm C}^{\rm SO} + \hat{H}_{\rm OH}^{\rm rotr} \tag{2.2}$$

of $\hat{H}^{\rm rotr}$ induces no coupling between basis states differing in Λ (this follows directly from the matrix representation in Hund's coupling case *b* applied to the Hill-van Fleck Hamiltonian, see, e.g., Ref. 49). On the other hand, $U^{\rm lr}$, in contrast to $U^{\rm ex}$ and $\hat{H}_{\rm C,OH}^{\rm rotr}$, is independent of spin variables.

In summary, $\hat{H}^{\rm rotr}$ in the present work is expressed by

$$\hat{H}^{\rm rotr} = U^{\rm lr} + U^{\rm ex} + \hat{H}_{\rm C}^{\rm SO} + \hat{H}_{\rm OH}^{\rm rotr} \tag{2.3}$$

which asymptotically, for $R \to \infty$, approaches $\hat{H}_{\rm C,OH}^{\rm rotr}$ from Eq. (2.2). The accurate quantum numbers of the free reactants then are the total angular momentum $J_{\rm C}$ ($J_{\rm C} = 0$, 1 and 2) of the C(^{3}P) manifold, its projection $M_{J_{\rm C}}$ onto the interreactant axis (directed from the center of mass of OH to the C atom), the total angular momentum $J_{\rm OH}$ of the OH($^2\Pi$, $J_{\rm OH}$) manifold ($J_{\rm OH}$ being either $J_{\rm OH}^-$ or $J_{\rm OH}^+$ for the F_1 or F_2 ladder of levels, respectively) with its projection $M_{J_{\rm OH}}$ onto the interreactant axis. To each state of the pair of quantum numbers $J_{\rm OH}^-$ and $J_{\rm OH}^+$ there belong two substates (conventionally called *e* and *f* states) that differ in parity. We consider these states as degenerate, i.e., we assume that the nonadiabatic coupling between these two states falls into the sudden regime. In this way, for $R \to \infty$, the asymptotic eigenvalues of $\hat{H}^{\rm rotr}$, $E_{\rm C,OH}^{\rm rotr}(J_{\rm C}, J_{\rm OH}^{\pm})$, are given by

$$\begin{aligned}
&E_{\rm C,OH}^{\rm rotr}(J_{\rm C}, J_{\rm OH}^{\pm}) = E_{\rm C}(J_{\rm C}) + E_{\rm OH}^{\rm rotr}(J_{\rm OH}^{\pm}),\\
&E_{\rm C}(J_{\rm C}) = aJ_{\rm C}(J_{\rm C}+1),\\
&E_{\rm OH}^{\rm rotr}(J_{\rm OH}^{+} = 1/2) = B - A,\\
&E_{\rm OH}^{\rm rotr}(J_{\rm OH}^{\pm} \geq 3/2) = B(J_{\rm OH}^{\pm} - 1/2)(J_{\rm OH}^{\pm} + 3/2) - A/2\\
&\quad \pm\sqrt{B^2(J_{\rm OH}^{\pm} - 1/2)(J_{\rm OH}^{\pm} + 3/2) + (B - A/2)^2},
\end{aligned} \tag{2.4}$$

where $a = 7.72\,{\rm cm}^{-1}$ is the Russell-Saunders spin-orbit coupling coefficient for the ^{3}P state of the C atom, $B = 18.55\,{\rm cm}^{-1}$ is the rotational constant of OH($^2\Pi$) in its ground vibrational state, and $A = -139.7\,{\rm cm}^{-1}$ is the spin-orbit coupling coefficient for OH($^2\Pi$), see Ref. 50. The order $a < B < |A|$ is responsible for specific temperature regimes of the capture process. The energy levels of the separated reactants, for non-rotating OH (NR) or for vanishing spin–orbit (no SO, NSO) interactions, are obtained from Eq. (2.4) by putting $B = 0$ or $a = A = 0$, respectively, i.e.,

$$\begin{aligned}
E_{\rm NR}^{\pm}(J_{\rm C}) &= aJ_{\rm C}(J_{\rm C}+1) \mp A/2 - A/2,\\
E_{\rm NSO}(K) &= E_{\rm OH}^{\rm rotr}\left(A = 0, J_{\rm OH}^{\pm} = K \pm 1/2\right)\\
&= B\left\{K(K+1) - 1\right\}.
\end{aligned} \tag{2.5}$$

The first line in Eq. (2.5) corresponds to the asymptotic energy levels of the eighteen MBO states, and the second line, with *K* being the quantum number of the total electronic rotational angular momentum of a rotor in a Π state, to the energy levels of a free OH molecule in the limit of Hund's coupling case *b* (spin uncoupled from the molecular axis).

The eigenvalues of the Hamiltonian $\hat{H}^{\rm rotr}$ in Eq. (2.3) can be calculated in matrix representation of any basis which is consistent with the approximation made for the asymptotic Hamiltonian $\hat{H}_{\rm C,OH}^{\rm rotr}$. Neglecting SO interactions, we chose to write the matrix $H^{\rm rotr}$ in the basis of the rotronic functions of the separated reactants as

$$\langle L, M_L, K, M_K, \Lambda, S, M_S| = \langle L, M_L|\langle K, M_K, \Lambda|\langle S, M_S| \tag{2.6}$$

with fixed rotronic moment *K* of OH, total spin *S* of the system, the projections M_K of *K*, M_S of *S*, M_L of the electronic moment $L = 1$ of C(^{3}P) onto the interreactant axis, and the projection $\Lambda = \pm 1$ of the electronic moment of OH($^2\Pi$) onto the molecular axis (details of the used frames and angular momentum projections are given in Subsection A 1 of the Appendix). We note here that, with the electronic component of this basis with reference to $U^{\rm lr} + U^{\rm ex}$, one obtains the correct symmetry representation of the electronic states of the adduct. However, because $\hat{H}_{\rm C,OH}^{\rm rotr}$ originally was written in the matrix representation of Hund's coupling case *a*, a transformation to the functions of Eq. (2.6) is required. Keeping in mind the different quantizations of the spins in the two basis sets (quantization onto molecular and interreactant axes), we formulate this transformation as

$$\begin{aligned}
&\langle J_{\rm C}, M_{J_{\rm C}}, J_{\rm OH}, M_{J_{\rm OH}}, \Omega|L, M_L, S, M_S, K, M_K, \Lambda\rangle\\
&= (-1)^{M_L(M_L+1)/2} C^{J_{\rm C}, M_{J_{\rm C}}}_{1, M_L 1, M_{J_{\rm C}} - M_L} C^{S, M_S}_{1, M_{J_{\rm C}} - M_L 1/2, M_S - M_{J_{\rm C}} + M_L}\\
&\quad \times \langle J_{\rm OH}, M_{J_{\rm OH}}, \Omega|D^{1/2}_{M_S - M_{J_{\rm C}} + M_L, \Omega - \Lambda}(\varphi, \theta, \chi)|K, M_K, \Lambda\rangle\\
&= (-1)^{M_L(M_L+1)/2}\\
&\quad \times \sqrt{\frac{2J_{\rm OH}+1}{2K+1}} C^{J_{\rm OH}, M_{J_{\rm OH}}}_{K, M_K 1/2, M_S - M_{J_{\rm C}} + M_L} C^{J_{\rm OH}, \Omega}_{K, \Lambda 1/2, \Omega - \Lambda}\\
&\quad \times C^{J_{\rm C}, M_{J_{\rm C}}}_{1, M_L 1, M_{J_{\rm C}} - M_L} C^{S, M_S}_{1, M_{J_{\rm C}} - M_L 1/2, M_S - M_{J_{\rm C}} + M_L}.
\end{aligned} \tag{2.7}$$

The C-factors here are the Clebsch–Gordan coefficients for angular momentum addition. The Wigner function $D(\phi,\theta,\chi)$ in Eq. (2.7), representing the rotation of the quantization axis of the spin, here is responsible for the transformation from half-integer momentum ($J_{\rm OH}$ in Hund's coupling case a) to integer momentum quantum number (K in Hund's coupling case b) rotronic functions. The integration variables in the calculation of the corresponding matrix element are the Euler angles φ, θ, χ for orientation of the body fixed system (with the molecular axis taken as the ζ-axis and the adduct plane taken as the reference $\xi\zeta$-plane) with respect to the space fixed system (with the reference xz-plane passing through the interreactant axis $\mathbf{R}$ taken as the z-axis, see Subsection A 1 of the Appendix).

The adiabatic channels are specified by the exact quantum numbers of total angular momentum and total parity (see, e.g., Refs. 20 and 51). In addition, they are characterized by a series of good quantum numbers such as the projection of the total momentum onto the collision axis,

$$P = M_L + M_K + M_S = N + M_S, \tag{2.8}$$

where N is the projection of the total rotronic momentum, and further quantum numbers for the numbering of states which asymptotically correspond to different quantum numbers of free OH as well as to different fine-structure components of free C (see Eq. (2.4)). In our approximation sub-matrices differing in P are uncoupled and can be diagonalized separately. States differing in the sign of P only are degenerate and do not need any separate consideration.

Three features of the matrix $H^{\rm rotr}$ appear worth mentioning in particular. First, in the region of large R, the matrix $H^{\rm rotr}$ approaching $H^{\rm rotr}_{\rm C,OH}$ remains non-diagonal in the adopted basis. Second, in the region of intermediate R, which is of particular importance for capture, the NBOAC potential curves exhibit a pattern of narrowly avoided crossings that originate from the coupling of the states with $\Lambda = \pm 1$ by the axially non-symmetric component of $U^{\rm lr}$. Since we here avoid the discussion of nonadiabatic effects caused by the translational motion, the passage across such narrowly avoided crossings may be considered for two limiting cases, the adiabatic and the diabatic regimes. This leads to two possibilities for correlations between the states of the adduct and the states of the separated reactants of a given P, see below. Third, in the region of small R, the pattern of the eigenvalues of $\hat{H}^{\rm rotr}$ reflects the importance of exponentially increasing $U^{\rm ex}$ and of diminishing SO interaction.

Employing an asymptotic approach to $\hat{H}^{\rm rotr}$ allows one to consider different types of non-BO couplings. The prize to pay for the asymptotic treatment then is the loss of an indication into which BO electronic state individual channels will lead at small R. We overcome this problem by following the channel potentials $V_i(R)$ to intermediate values of R where the BO states have separated sufficiently. For this range, we then compare AC potentials on the various levels (BO, NBO(NSO), and NBO) which allows us to specify which electronic state of the adduct is finally reached. For instance, we calculate NBO(NSO) states as eigenvalues of $\hat{H}^{\rm rotr}$ neglecting SO interactions ($a = A = 0$) and replacing the component $\hat{H}^{\rm rotr}_{\rm C,OH}$ by the operator $B(\hat{\mathbf{K}}^2 - \Lambda^2)$ (see, e.g., Ref. 49). These states then are specified by the good quantum numbers S, M_S, and N. Finally, we solve the electronic MBO problem, i.e., we determine the eigenvalues of $U^{\rm lr} + U^{\rm ex}$ in the basis of the electronic functions

$$\langle L, M_L, \Lambda, S, M_S| = \langle L, M_L|\langle\Lambda|\langle S, M_S|. \tag{2.9}$$

The diagonalization of the corresponding interaction matrix altogether leads to 12 electronic states of the adduct, 3 of ^{2}A′, 3 of ^{2}A″, 3 of ^{4}A′, and 3 of ^{4}A″ symmetry where the lowest state of ^{2}A′ symmetry is the ground electronic state (X^2A') of the adduct. For each of the corresponding PESs, we then construct adiabatic channels as solutions of the hindered rotor problem. We do this for $\hat{H}^{\rm rotr}$ replacing its component $\hat{H}^{\rm rotr}_{\rm C,OH}$ by the kinetic energy operator $B\hat{\mathbf{J}}^2_{\rm rot}$ of a structureless free linear rotor and employing a matrix representation with spherical harmonics

$$\langle J_{\rm rot}, M| = Y^{J_{\rm rot}}_M(\theta,\varphi)\,. \tag{2.10}$$

Here M is the projection of the rotational angular momentum onto the interreactant axis and θ and φ are the polar and azimuthal spherical coordinates of the rotor in the space fixed system (see Table I in Subsection A 1 of the Appendix). Due to the axial symmetry, the projection M is a good quantum number. Along with the classification by S, M_S, and the symmetry properties of the electronic states of the adduct, the NBO ACs are characterized by the good quantum number M. Because the projection of the total electronic moment of the adduct averages to zero, the projection quantum number M obeys the correlations

$$\begin{aligned} N &= M, \\ P &= M + M_S. \end{aligned} \tag{2.11}$$

Taking into account the correlation rules of Eqs. (2.8) and (2.11), we may separate the AC states, calculated in BO, NBO(NSO), and NBO approximations, into groups of fixed $|P|$. We do this at fixed R in the intermediate range, for the C + OH system, e.g., at $R = 5$ a.u. Inside these groups we correlate AC states in the order of increasing energy one after the other, from BO to NBO(NSO) and then from NBO(NSO) to NBO. This specifies which BO electronic state will be reached by individual NBO ACs. We remember that a similar type of correlation was employed in the earlier versions of the SACM, see, e.g., Ref. 6. We note that the energy mismatch at $R = 5$ a.u., at least for the lowest BO, NBO(NSO), and NBO AC states, is found to be small in comparison to the energy quantum of the hindered rotation. Our procedure thus is expected to provide a reasonable method to determine the branching of reactive fluxes into various electronic states of the adduct.

B. Potential energy surfaces at long range

As long as the SO interaction is not considered, calculations using the basis of the electronic functions of the C($2p^2$, ^{3}P) + OH($1\pi^3$,$^2\Pi$) manifolds result in six doublet and six quartet adduct states. Asymptotically, for $R \to \infty$, the twelve PESs then converge to a single energy level that corresponds

to C(P) and to non-rotating OH(Π). Within this approximation we begin with the construction of a matrix representation for $\hat{H}^{\rm rotr} - \hat{H}^{\rm rotr}_{\rm C,OH}$, i.e., for $U^{\rm lr} + U^{\rm ex}$, which is written in the basis of the electronic wave functions (2.9). The long-range interaction $U^{\rm lr} = U^{\rm elst} + U^{\rm ind} + U^{\rm disp}$ in our asymptotic approach is represented by a series expansion of the multipole electrostatic, $U^{\rm elst}$, induction, $U^{\rm ind}$, and dispersion, $U^{\rm disp}$ interactions up to R^{-6} terms, while the exchange interaction $U^{\rm ex}$ has its asymptotic two-electron form. Details of the calculation of the various contributions to $U^{\rm lr}$ at long range are given in Subsection A 2 of the Appendix.

At large R, all terms of $U^{\rm lr}$ except the dipole–quadrupole contribution can be neglected and the results of the diagonalization converge to three, 12-fold degenerate, PESs with R^{-4} dependence,

$$E_{\rm X,2}(R,\theta) = -3\sqrt{2}d\langle r_{\rm C}^2\rangle\left(\sqrt{2}\cos\theta \pm \sqrt{13+5\cos 2\theta}\right)/20R^4,$$
$$E_1(R,\theta) = 3d\langle r_{\rm C}^2\rangle\cos\theta/5R^4, \tag{2.12}$$

where atomic units (a.u.) are used, $\langle r_{\rm C}^2\rangle = 3.89$,[50] $d = 0.702$ (see Table II in Subsection A 2 of the Appendix), and where the subscripts X (+ sign in the parenthesis), 1, and 2 (− sign in the parenthesis) correspond to the ground, first and second excited electronic states, respectively. (Contributions from terms proportional to R^{-5} as well as induction ($U^{\rm ind}$) and dispersion ($U^{\rm disp}$) terms proportional to $R^{-6}$are given in Table S.1 of the supplementary material.[60]) We note that our long-range expressions for $U^{\rm lr}$ agree with the results of Ref. 28, see Table III in Subsection A 2 of the Appendix.

As emphasized above, a central element of our treatment is the inclusion of the asymptotic exchange interaction $U^{\rm ex}$. As this inclusion has not been performed before, it will be described in the following. Further details are given in Subsection A 3 of the Appendix. We retain four components of the exchange between the valence and the first upper inner shells. These asymptotic exchange components (see Eq. (27) from Ref. 32 and Eqs. (18) and (19) from Ref. 57) are determined by the asymptotic radial behavior of the valence 2p (q = 1) and inner 2s (q = 3) atomic orbitals of C($2s^2 2p^2$,^{3}P) and the valence 1π (q = 2) and upper inner 3σ (q = 4) molecular orbitals of OH($3\sigma^2 1\pi^3$,$^2\Pi$) (the molecular orbitals being approximated by atomic 2p-orbitals centered at the center-of-mass of OH close to the nucleus of O). The corresponding radial wave functions are expressed as

$$\psi_q\left(n=2,\ l=0,\ 1;\ \ \gamma_q r \gg 1\right) = A_q r^{1/\gamma_q - 1}\exp(-\gamma_q r)$$
$$\times\left\{1 - \frac{1}{2\gamma_q^2 r}\left(\frac{1}{\gamma_q} - 1\right) + \frac{l\,(l+1)}{2\gamma_q r} + O\left(\frac{1}{r^2}\right)\right\},$$
$$\gamma_q = \sqrt{2\varepsilon_q}, \tag{2.13}$$

where n and l are principal and azimuthal quantum numbers of the atomic orbitals. The energies ε_q of the valence orbitals in Eq. (2.13) correspond to the first ionization potentials; in the molecular case they are given by the first vertical ionization potentials (ionization starting at fixed O–H distance $r_{\rm OH} = \langle r^{\rm OH}_{\rm v=0}\rangle$, averaged over the ground vibrational state of OH). For the inner orbitals, in addition to the ionization potential, ε_q includes the energy of the cationic excitation, arising from the filling of the hole in the valence shell with an electron from the parent inner shell (i.e., by the excitation $C^+(^2P \rightarrow {}^4P)$[50] or by the vertical excitation $OH^+(X^3\Sigma^- \rightarrow 1^3\Pi)$[58]). Matching the *ab initio* orbitals (see, e.g., Ref. 53) with their asymptotic form of Eq. (2.13), defines the coefficients A_q. For example, this gives A_1(C, $2p^2$) = 1.3[50] and A_2(OH,$1\pi^3$) = 1.3[32] (in Ref. 59 the coefficient A_2(OH, $1\pi^3$) was taken as the coefficient A_1(O, $2p^4$) which, according to Ref. 50, is equal to 1.3). Keeping the definition of the orbital energies ε_q as given above, we slightly modified the coefficients A_q in order to improve the match between our asymptotic and the *ab initio* PESs of Refs. 26 and 29. The parameters which we substitute into Eq. (2.13) for this purpose are listed in Table IV of Subsection A 3 of the Appendix.

Considering the angular dependence of the molecular orbitals (approximated by spherical harmonics), one has to take into account their quantization along the molecular axis. The passage to the quantization along the interreactant axis generates sums of products of the transformed orbitals for "outgoing" and "incoming" exchange electrons over projection quantum numbers, which contain as coefficients the products of the corresponding Wigner D-functions of the Euler angles for axis rotation. We reduce these coefficients to finite Clebsch-Gordan sums of Wigner D-functions which considerably simplifies further calculations of the rotronic matrix elements. The atomic (or molecular) orbital approximation reduces the electronic wave function to a sum of products of one-electron orbital and moiety functions (for the nomenclature see Ref. 56). The factors arising for OH here are the coefficient of the fractional parentage of the OH^+ moiety, $G^{S_{\rm OH}\ \ Q_{\rm OH}}_{S_{\rm OH^+}\ \ Q_{\rm OH^+}}$, the Clebsch-Gordan coefficient of the electron and the OH^+ moiety spin addition, $C^{S_{\rm OH} M_{S_{\rm OH}}}_{S^+_{\rm OH} M_{S^+_{\rm OH}}\, 1/2\, m_s}$, and the molecular Clebsch-Gordan coefficient of the electronic momentum addition, $[^{Q_{\rm OH^+}\ \lambda\ Q_{\rm OH}}_{\Lambda_{\rm OH^+}\ \tilde{\lambda}\ \Lambda_{\rm OH}}]$. For example, the factor for the parent OH($1\pi^3\ ^2\Pi$) and the moiety $OH^+(1\pi^2\ ^3\Sigma^-)$ molecular configurations consists of the coefficients

$$G^{1/2\ \ 1}_{1\ \ 0^-} = \frac{1}{\sqrt{2}}, \quad C^{1/2\, M_{S_{\rm OH}}}_{1 M_{S_{\rm OH^+}}\, 1/2\, m_s}, \quad \begin{bmatrix} \Sigma^- & 1 & 1 \\ 0 & \Lambda & \Lambda \end{bmatrix} = -1. \tag{2.14}$$

For the calculation of the electronic matrix elements of $U^{\rm ex}$, we follow a formalism which reduces the total spin matrix representation of the Dirac operator in the Heitler-London exchange Hamiltonian (with the components $\langle S, M_S|$ from Eq. (2.9)) to the individual reduced matrix elements of spins of the exchanged electrons (see Ref. 57).

Within our approach, the exchange interaction can be expressed through the exchange integral functions $I^{(q,q')}_{kn}$. The latter are given by an integral representation (see, e.g., Ref. 56), and can be easily calculated numerically. We have fitted them, within the range of R from 4 to 10 a.u., by an expression

$$\ln\left(I^{(q,q')}_{kn}\right) = a^{(q,q')}_{kn} R^3 + b^{(q,q')}_{kn} R^2 + c^{(q,q')}_{kn} R + d^{(q,q')}_{kn} \tag{2.15}$$

with fitting coefficients listed in Table V of Subsection A 3 of the Appendix.

Having constructed the long-range expressions for $U^{\rm lr}$ and $U^{\rm ex}$, PESs in the absence of SO interaction are obtained by diagonalization of the electronic Hamiltonian matrix

$$H^{\rm el}_{\rm NSO} = \langle L, M_L, \Lambda, S, M_S | U^{\rm lr} + U^{\rm ex} | L', M'_L, \Lambda', S, M_S \rangle \tag{2.16}$$

which generates 12 PESs of the adduct, 3 of ^{2}A′, 3 of ^{2}A″, 3 of ^{4}A′, and 3 of ^{4}A″ symmetry. We observe that the described asymptotic theory at intermediate interaction distances, $4 < R < 7$ a.u., nearly quantitatively reproduces the *ab initio* calculations of the lowest 4 PESs of each spin and reflection symmetry of the adduct from Refs. 26 and 29. (This is illustrated in Fig. 8 in Subsection A 3 of the Appendix, see also Fig. S.1 of the supplementary material.[60]) Therefore, we can be confident about the quality of the asymptotic PESs generated in the described way and we can use these PESs to construct BO ACs. This will be described in Sec. III.

When the SO interaction is switched on, the total spin S and its projection M_S cease to be good quantum numbers. In states with given $J_{\rm C}$ and Ω, the SO interaction asymptotically reduces to the sum of the SO interactions of the free reactants, see Eq. (2.5). To solve the electronic problem in this case, we transform the matrix representation of $U^{\rm lr} + U^{\rm ex}$, as written in the basis of the functions of Eq. (2.9), to a basis of eigenfunctions $\langle J_{\rm C}, M_{J_{\rm C}}, \Omega|$ for the total SO interaction:

$$\begin{aligned}
&\langle J_{\rm C}, M_{J_{\rm C}}, \Omega | L, M_L, \Lambda, S, M_S \rangle \\
&\quad = (-1)^{M_L(M_L+1)/2} \\
&\qquad \times C^{J_{\rm C}, M_{J_{\rm C}}}_{1, M_L\ 1, M_{J_{\rm C}} - M_L} C^{S, M_S}_{1, M_{J_{\rm C}} - M_L\ 1/2, M_S - M_{J_{\rm C}} + M_L} \\
&\qquad \times d^{1/2}_{M_S - M_{J_{\rm C}} + M_L, \Omega - \Lambda}(\theta)\,.
\end{aligned} \tag{2.17}$$

Here the Wigner $d(\theta)$-functions correspond to the rotation from the interreactant to the molecular quantization axis of the molecular spin $S_{\rm OH} = 1/2$. The diagonalization of the electronic Hamiltonian matrix (for $E^{\pm}_{\rm NR}(J_{\rm C})$ see Eq. (2.5)),

$$\begin{aligned}
H^{\rm el} &= \langle J_{\rm C}, M_{J_{\rm C}}, \Omega | U^{\rm lr} + U^{\rm ex} | J'_{\rm C}, M'_{J_{\rm C}}, \Omega' \rangle \\
&\quad + \delta_{J'_{\rm C}, J_{\rm C}} \delta_{M'_{J_{\rm C}}, M_{J_{\rm C}}} \delta_{\Omega', \Omega} E_{\rm NR}(J_{\rm C}, \Omega), \\
E_{\rm NR}(J_{\rm C}, \Omega = \pm 3/2) &= E^{-}_{\rm NR}(J_{\rm C}), \\
E_{\rm NR}(J_{\rm C}, \Omega = \pm 1/2) &= E^{+}_{\rm NR}(J_{\rm C})
\end{aligned} \tag{2.18}$$

generates 18, according to Kramers doubly degenerate, PESs of COH (see, e.g., Ref. 32). Contour plots of the 2 lowest PESs are shown in Fig. 1 (contour plots for the next 4 higher PESs are shown in Figs. 9 and 10 in Subsection A 3 of the Appendix). The solid and dashed lines correspond to equipotential lines of the PESs from asymptotic theory, for positive and negative energies, respectively. The figure in addition includes gray lines which indicate the distance between the displayed and the next higher PESs. Locations with distances less than 0.1 B correspond to places where non-BO dynamic behavior becomes most probable. Inside the central parts, $R \le 5$ a.u., the figure also specifies which PESs without SO-coupling in the intermediate range correspond to the displayed PES including SO-coupling. The figure illustrates the complicated structure of the crossing of the BO PESs. A similar behavior was documented for the PESs of the OH + O system in Ref. 32 and it is expected to be encountered quite generally. Although NBO ACs in the present work are generated by direct diagonalization of $\hat{H}^{\rm rotr}$ (as described in Sec. III), their BO counterparts including SO-coupling could also be generated employing the PESs of Fig. 1. We do not follow this concept in the present work, because BO ACs including SO-coupling would not lead to the correct rotronic correlations at long distances such that no advantage would be gained.

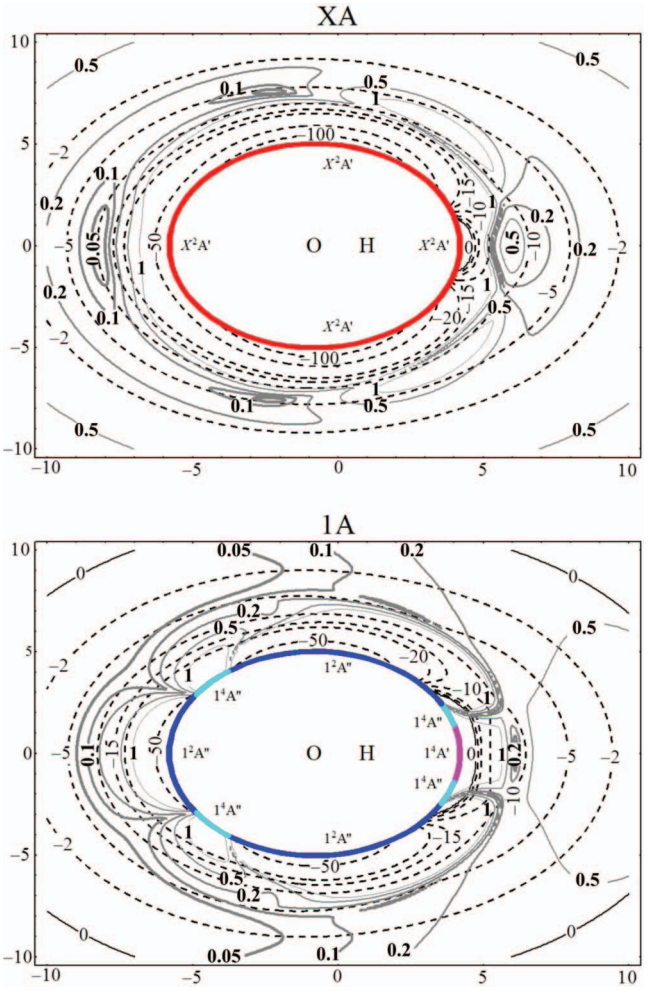

FIG. 1. Contour plots of the PESs for the two lowest electronic states of the adduct (calculations including SO-coupling; OH oriented along the horizontal axis with its geometric center at the origin, position of C in the plane with distances from the origin in a.u., O–H distance = 1.85 a.u.; energies in units of B, the gray contour lines give the energetic distance to the next higher PES; the color- coded lines specify the electronic correlation with NSO states).

It appears worthwhile to remember that PESs, which asymptotically correlate with the fine-structure state $J_{\rm C} = 0$ of the free C atom (having neither an atomic quadrupole moment, nor an anisotropic component of the polarizabilities), are of R^{-6} long-range character. The asymptotic continuation of the *ab initio* PES of ground state COH(X^2A') from Ref. 26, such as used in the CT calculations of Ref. 27, also reduces to this form and takes the value $V(R) = -97.3\ R^{-6}$ (we here extracted the coefficient from the rate constant at the lowest temperature of 5 K which was given in Ref. 27). We note that

the coefficient exceeds more than twice the values for the total isotropic induction and dispersion coefficients (41.4 for $M_L = \pm 1$, $L_b = 0$ and 39.3 for $M_L = 0$, $L_b = 0$, see Subsection A 2 of the Appendix and Ref. 28). This discrepancy is essentially the result of second order contributions to the PES from the electrostatic interaction (being proportional to R^{-8}, see below) which were neglected in Ref. 27.

III. BO, NBO(NSO), AND NBO CALCULATIONS OF ADIABATIC CHANNEL POTENTIALS FOR THE C + OH SYSTEM

In earlier versions of the SACM, for processes with loose transition states involving reactants with closed electronic shells (see Refs. 5, 6, and 8–12), it was sufficient to calculate AC potentials not too far inside the centrifugal barriers. For low temperatures, this corresponded to rather large distances R. In the present formulation of an SACM for reactants with open electronic shells, AC energies have to be followed to much smaller R (here we consider values of R down to 5 a.u.) where the PESs of different electronic states separate from each other sufficiently and an electronic assignment of the NBO ACs via a comparison with NBO(NSO) and BO ACs becomes possible. For the present applications such as described in Sec. II, the asymptotic theory including exchange interaction covers well the relevant range of distances. Different from the earlier versions of the SACM, however, all NBO AC potentials now are obtained by direct diagonalization of the rotronic Hamiltonian without passing through PES calculations. BO AC potentials, on the other hand, are calculated as before by diagonalization of the hindered rotor Hamiltonian on the precalculated PES. We pay particular attention to the behavior of the lowest BO, NBO(NSO), and NBO AC potentials at large distances because these determine the low temperature (semi-classical) limit of the corresponding capture rate constants.

We first consider BO ACs. When SO and the rotronic interaction inducing A′/A″ state mixing are switched off, adiabatic channels divide into independent groups of BO channels. These differ both in their electronic state (subscript ε) and in the projection quantum number M of the rotational momentum $J_{\rm rot}$ of the rotor onto the interreactant axis. At values of R in the interval 5–40 a.u., we fit axially symmetric asymptotic PESs (for the lowest ones, see Fig. 8 in Subsection A 3 of the Appendix) as functions of the polar angle θ and expand them into Legendre polynomials. We then solve the secular problem for the hindered rotor Hamiltonian matrix

$$\begin{aligned} H^{\rm rot} &= \delta_{J'_{\rm rot},J_{\rm rot}} B J_{\rm rot}(J_{\rm rot}+1) \\ &\quad + \langle J_{\rm rot}, M|E_\varepsilon(R,\theta)|J'_{\rm rot}, M\rangle, \\ E_\varepsilon(R,\theta) &= \sum_n c_n(R) P_n(\cos\theta), \end{aligned} \tag{3.1}$$

written in the representation of the spherical harmonics of Eq. (2.10). As the result we obtain the BO adiabatic channel potentials $V^{(\varepsilon)}_{M,i}(R)$. For the lowest BO adiabatic channel potential in the electronic ground state X^2A', the asymptotic dependence on R is given by the diagonal matrix element of the asymptotic interaction $E_X(R,\theta)$ from Eq. (2.12), i.e.,

$$\begin{aligned} V^{(X)}_{M=0,i=0}(R) &= \langle J_{\rm OH}=0, M=0|E_X(R,\theta)|J_{\rm OH}=0, M=0\rangle \\ &= -\frac{3d\langle r_C^2\rangle}{20R^4}\left(3+\frac{1}{\sqrt{5}}\ln\left[\frac{47+21\sqrt{5}}{2}\right]\right) \end{aligned} \tag{3.2}$$

(as before in a.u., with $d = 0.702$ and $\langle r_C{}^2\rangle = 3.89$, see Subsection A 2 of the Appendix).

We next consider ACs in the NBO(NSO) approximation, which accounts for the A′/A″ state mixing. The projection N (asymptotically equal to $M_L + M_K$ and, according to Eq. (2.11), correlating with M in the intermediate range of R) of the total angular electronic and rotational (rotronic) momentum onto the interreactant axis remains a good quantum number. As long as the SO interaction is switched off and the total spin S is a good quantum number, also its projection M_S onto the interreactant axis is a good quantum number leading, like in the BO approximation, to an additional degeneracy only. The matrix representation for the rotronic problem at given N in this case uses the basis functions from Eq. (2.6),

$$\begin{aligned} &\langle L, M_L, K, N-M_L, \Lambda, S, M_S| \\ &\quad = \langle L, M_L|\langle\Lambda|\langle K, N-M_L, \Lambda|\langle S, M_S|, \\ &\langle K, N-M_L, \Lambda| = \sqrt{(2K+1)/4\pi}\, D^K_{N-M_L\,\Lambda}(\varphi,\theta,\chi) \end{aligned} \tag{3.3}$$

which are quantized both along the fixed interreactant and rotating molecular axes (the angle χ here is not specified and can be put to equal to zero). The solution of the corresponding secular problem, for the 18-fold degenerate lowest states with $K = 1$ (spin degeneracy here is excluded), in the limit of large R leads to the asymptotic AC potentials given in Table VI in Subsection A 4 of the Appendix. The close match of the NBO(NSO) and BO states with $M = N$ at $R = 5$ a.u. indicates that only one of the two repulsive channels with $N = 0$ (written in parenthesis in Table VI in Subsection A 4 of the Appendix) leads into the $1^2A''$ electronic state, while all others lead into the X^2A' state.

We finally proceed to the calculation of NBO adiabatic channel potentials, with SO-coupling switched on and keeping the basis of Eq. (2.6). This basis was already employed for the interaction $U^{\rm lr} + U^{\rm ex}$, when the matrix representation of the Hamiltonian $\hat{H}^{\rm rotr}$ in the NBO(NSO) approximation was constructed. We now apply the transformation of Eq. (2.7) to this basis with respect to the matrix $H^{\rm rotr}_{\rm C,OH}$ of Eq. (2.2) which originally was written in the representation of Hund's coupling case a. According to the angular momentum addition rules, it requires large (but finite) numbers of functions to reproduce that part of the energy spectrum of the reactants (up to about $5 - 7\,k_BT$) which contributes to the low-temperature capture rate constant. The half-integer projection P of the total angular momentum onto the interreactant axis here exclusively survives as a good quantum number and it characterizes the energy eigenvalues $V_{|P|,i}(R)$ (in the approximation of fixed interreactant axis these are doubly degenerate with respect to the sign of P).

Using the correlation rules for the angular momentum projections (see Eqs. (2.8) and (2.11)), we now establish

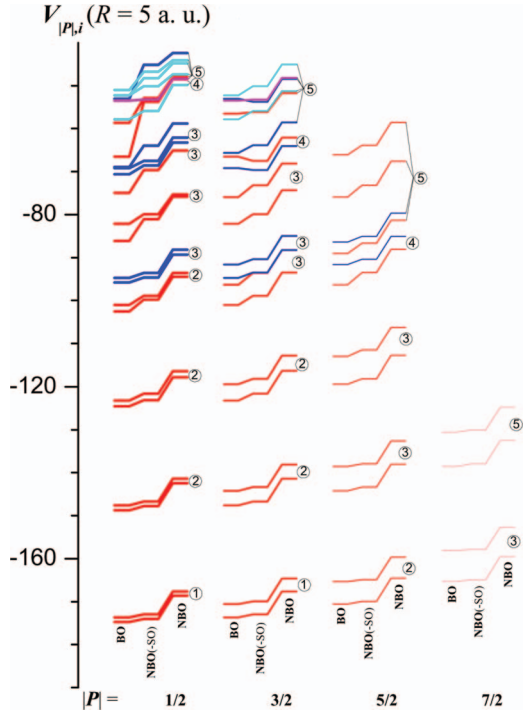

FIG. 2. Energies of the lowest ACs at $R = 5$ a.u. in BO, NBO(NSO), and NBO approximation (ACs leading into X^2A' (—, red), $1^2A''$ (—, blue), $1^4A'$ (—, pink), and $1^4A''$ (—, cyan); encircled numbers indicate the number of the original state at $R \to \infty$, e.g., ① at 1.8 B, ② at 2.6 B, see Fig. 3).

within groups of the same $|P|$ the sequence of the BO, NBO(NSO), and NBO adiabatic channel states at $R = 5$ a.u. (from BO to NBO(NSO) and then from NBO(NSO) to NBO). Together with the calculation of the NBO AC potentials, this allows us to specify the "entrance states" of the free reactants with respect to their branching into the different electronic states of the adduct. The procedure and the results of this specification are illustrated in Figs. 2 and 3, respectively. Fig. 2 shows AC energies, at fixed $R = 5$ a.u., for large amplitude bending (hindered rotation) of the adduct, calculated at the three levels of approximation, BO, NBO(NSO), and NBO. When the level of approximation for the shown states is increasing, the trends are very regular and the influence of adding interactions is easily recognizable. Our procedure thus clearly provides the electronic state assignment of the adduct vibronic states at intermediate (NBO(NSO)) and at the highest (NBO) levels of approximation. The choice of 5 a.u. as a BO-NBO matching distance was justified by the fact that the different BO electronic states at this distance are sufficiently separated. At smaller distances, the increasing interaction of the molecular modes finally leads to the limits of applicability of the asymptotic theory and of the SACM procedure. These natural limitations of the procedure determining electronic branching become increasingly more serious for capture into higher electronic states and for higher temperatures.

Fig. 3 indicates the distribution of ACs, originating from the shown "entrance states" of the separated reactants, over the various BO states of the adduct. g_{rotr} denotes the corresponding number of ACs. One observes that only ACs with entrance energies $E_{entr} < 3B$ exclusively lead into the X $^2A'$ electronic ground state of the adduct. ACs with larger entrance energies show an increasing branching also into excited electronic states of the adduct. The branching is illustrated by the same color code in Figs. 2 and 3. Fig. 4 finally illustrates the difference between the branching of entrance states into the adduct X^2A' state within the present AC procedure (upper panel) and within the conventional electronic correlation between the lowest electronic state of the adduct and the lowest electronic state of the free reactants (lower panel). The red color here corresponds to branching into X^2A', the gray color to branching into excited electronic states. For example, in the conventional treatment the lowest states with $J_C \neq 0$ are closed for branching into X^2A' (this corresponds to a closure of 24 and 26 ACs starting from the entrance states at 2.5 B and 4.4 B, respectively) while they are open in the present procedure.

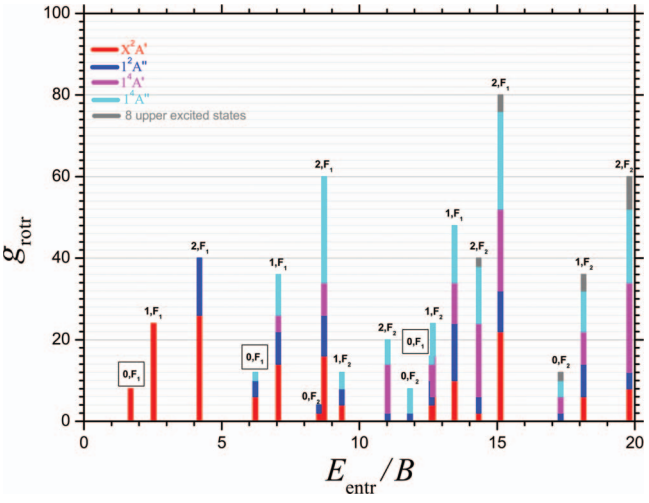

FIG. 3. Separated reactant states ($R \to \infty$) and their branching into ACs leading into different electronic states of the adduct (degeneracy g_{rot}; color code as in Fig. 2, higher states in gray, the two lines near 12.7 B nearly coincide).

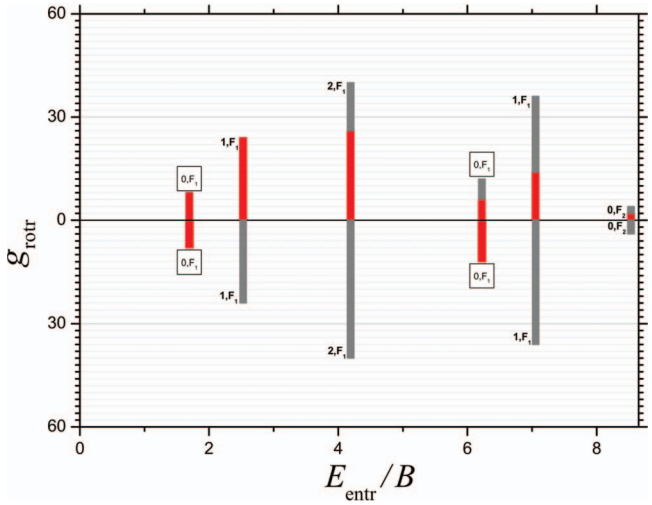

FIG. 4. As Fig. 3, red: formation of the electronic ground states of the adduct; gray: formation of excited electronic states (upper panel: present NBO approach, lower panel: conventional SBO approach).

Fig. 2 illustrates the values of selected AC potential curves $V_i(R)$ at $R = 5$ a.u. and their variation at the three levels of approximation (BO, NBO(NSO), and NBO). We do not show here examples of complete AC potential curves $V_i(R)$ because they look quite similar as the corresponding curves of other systems, e.g., as shown for $H + O_2$ in Ref. 14. Likewise the interplay between the $V_i(R)$ and the orbital energies T_{nuc}^{rot}, which leads to the centrifugal maxima $E_{0,i}(\ell)$ of the AC potential curves, resembles the illustrations of Ref. 14. Furthermore, the number of relevant channels in the present case is quite large such that their representation does not increase insight. Instead, in the following we only inspect the lowest AC potentials, as the low temperature (semi-classical) limit of the capture rate constant is completely determined by the long-range potentials of the 4 doubly degenerate adiabatic channels with $|P| = 1/2, 3/2$ (correlating with the lowest rotronic state $0, ^2\Pi_1$ ($J_C = 0$, $J_{OH}^- = 3/2$) of the free reactants). All of these adiabatic channels lead into the ground electronic state of the adduct (see Figs. 2–4).

Because of the spherical isotropy of the wave function, the atomic state with $J_C = 0$ possesses neither a quadrupole moment, nor an anisotropic component of the atomic dipole polarizabilities. As a consequence, the adiabatic channels at long range are 4-fold degenerate and their potentials can be represented by the expressions

$$\begin{aligned} {}^6V_{|P|=\frac{3}{2}} &= -C_{6,3/2}R^{-6} = -42.2R^{-6}, \\ {}^6V_{|P|=\frac{1}{2}} &= -C_{6,1/2}R^{-6} = -39.2R^{-6}, \end{aligned} \tag{3.4}$$

where the C_6-coefficients are given in detail in Table VII in Subsection A 4 of the Appendix. In the absence of diagonal matrix elements in the lowest rotronic state, there are nevertheless non-diagonal matrix elements of the atomic quadrupole moment. The dipole-quadrupole coupling with the upper states with $J_C = 2$ and $J_{OH} = 3/2$, 5/2 then is responsible for a second order perturbation of the considered lowest states (we limit ourselves here to the approximation of Hund's coupling case *a*):

$$\begin{aligned} {}^8V_{|P|=\frac{3}{2}} &= -C_{8,3/2}R^{-8} = -1.05 \times 10^4 R^{-8}, \\ {}^8V_{|P|=\frac{1}{2}} &= -C_{8,1/2}R^{-8} = -0.671 \times 10^4 R^{-8}, \end{aligned} \tag{3.5}$$

where the C_8-coefficients again are given in detail in Table VII of Subsection A 4 of the Appendix. These contributions deserve particular attention, because they contribute to capture rate constants in the temperature range considered below. In the presence only of R^{-6} terms, the capture rate constants would be proportional to ${C_6}^{1/3}$. Instead of numerically calculating k_{cap} for ACs with R^{-6} and R^{-8} contributions, we chose a simpler approach. We noted that the main contributions to k_{cap} come from values of $R = R_{eff}$ where $V(R_{eff}) = -C_6 {R_{eff}}^{-6}$ is about equal to $k_B T$. Modifying $C_6 {R_{eff}}^{-6}$ by $C_6 {R_{eff}}^{-6} + C_8 {R_{eff}}^{-8}$ and expressing this by $\bar{C}_6(T) {R_{eff}}^{-6}$ leads to a temperature dependent effective

$$\bar{C}_6(T) = \left\{ \frac{\sqrt[3]{C_{6,1/2}(T)} + \sqrt[3]{C_{6,3/2}(T)}}{2} \right\}^3 \tag{3.6}$$

to be used in the calculation of k_{cap}. With the additional contributions from Eq. (3.5), the effective parameter $\bar{C}_6(T)$ achieves its highest value of ≈80 at a temperature near $T = 2.5$ K. This value of $\bar{C}_6$ is twice the total induction and dispersion value of the channels (see Eq. (3.4)) and it accidentally is close to the value of C_6 obtained by the analytical isotropic continuation of the *ab initio* PES of Ref. 26 in Ref. 27 and employed in the CT calculations of k_{cap} in Ref. 27. A comparison with the CT results from Ref. 27 thus is of interest, see below.

IV. CALCULATION OF THERMAL CAPTURE RATE CONSTANTS FOR C + OH

Once the AC potential curves $V_i(R)$ and their channel maxima $E_{0,i}(l)$ are determined, one proceeds to the implementation of the latter quantities into expressions for kinetic observables like k_{cap} such as this is done in the various applications of SACM the usual procedure of SACM (Refs. 6–20). For example, one determines numbers of open channels $W(E,l)$ (i.e., numbers of ACs for which $E > E_{0,i}(l)$) or activated complex partition functions Q^* defined by

$$Q^* = \sum_{i,\ell} (2\ell + 1) \exp[-E_{0,i}(\ell)/k_B T], \tag{4.1}$$

where the $E_{0,i}(\ell)$ are the maxima of $V_i(R) + \hbar^2 \ell(\ell+1)/2\mu R^2$. The thermal rate constant for capture, $k_{cap}(T)$, in the nomenclature of transition state theory then is expressed by

$$k_{cap}(T) = \frac{k_B T}{h} \left(\frac{h^2}{2\pi \mu k_B T} \right)^{3/2} \frac{Q^*}{Q} \tag{4.2}$$

with Q^* and the corresponding product of reactant partition functions Q (unless stated differently, we use CGS units in this section). First, we only consider capture into the X^2A' electronic ground state of the adduct, characterized by $k_{cap,X}(T)$. Both Q^* and Q include rotronic states, the former of the activated complex, the latter of the reactants. Within our NBO treatment, Q_X^{*NBO} is given by

$$Q_X^{*NBO} = \sum_i g_i^X \sum_\ell (2\ell + 1) \exp\left[-E_{0,i}^X(\ell)/k_B T\right], \tag{4.3}$$

where the $E_{0,i}^X(\ell)$ are $V_i^X(R) + \hbar^2 \ell(\ell+1)/2\mu R^2$ are for a given adiabatic channel (i) leading into the adduct electronic ground state X^2A' (g_i^X is its degeneracy). The corresponding partition function Q of the free reactants here is given by

$$Q^{rotr}(T) = \sum_{J_C, J_{OH}^\pm} g(J_C, J_{OH}^\pm) \exp\left[-E_{C,OH}^{rotr}(J_C, J_{OH}^\pm)/k_B T\right], \tag{4.4}$$

where the summation includes all possible values of the rotronic quantum numbers J_C, J_{OH}^-, and J_{OH}^+ (see Eq. (2.4)). Inserting Q_X^{*NBO} and Q^{rotr} into Eq. (4.2), for Q^* and Q, respectively, gives the NBO rate constant for capture into the X^2A' state, denoted by $k_{cap,X}^{NBO}(T)$. Figs. 5 and 6 show the results. $k_{cap,X}^{NBO}(T)$ increases with temperature until a maximum is reached at 28 K. The subsequent decrease is slow, one half of the maximum value of 4.1×10^{-10} cm^{3}s^{-1} is attained only near 220 K.

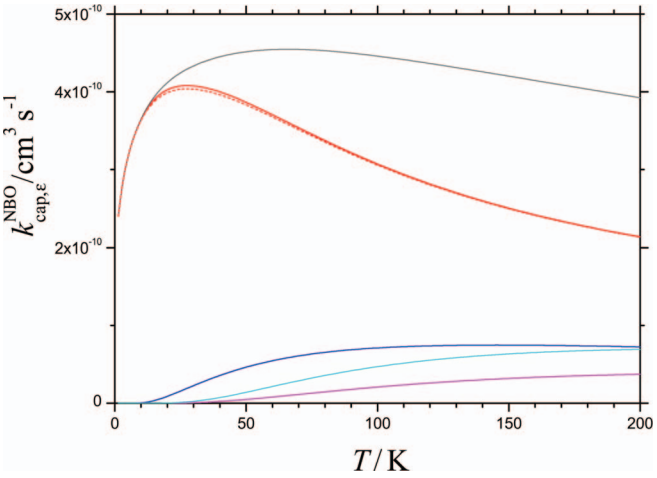

FIG. 5. Thermal capture rate constants $k^{\mathrm{NBO}}_{\mathrm{cap},\varepsilon}$ of C and OH into different electronic states ε of the adduct (—, red: into ground state, $\varepsilon = \mathrm{X}^2\mathrm{A}'$, with adiabatic (or —-, red dashed: with diabatic) passage through narrowly avoided crossings, see Sec. IV; —, blue; —, pink; and —, cyan: into $\varepsilon = 1^2\mathrm{A}''$, $1^4\mathrm{A}'$, $1^4\mathrm{A}''$ states of the adduct, respectively; —, gray: total rate constant for capture into the lowest four electronic states of the adduct).

With the AC potentials $\propto R^{-6}$ from Eq. (3.4), the limiting low temperature (semi-classical) capture rate constant according to the relation

$$k_{\mathrm{cap}} = 2^{11/6}\Gamma(2/3)\sqrt{\pi/\mu}C_6^{1/3}T^{1/6} \tag{4.5}$$

would be given by

$$k_{\mathrm{cap}}(T \to 0\,\mathrm{K}) = 1.92 \times 10^{-10}(T/\mathrm{K})^{1/6}\,\mathrm{cm}^3\mathrm{s}^{-1}. \tag{4.6}$$

As indicated above, however, the additional R^{-8} terms of Eq. (3.5) for the lowest ACs make a non-negligible contribution for intermediate temperatures (in the present case in the range 1–10 K), before the influence of higher ACs takes over

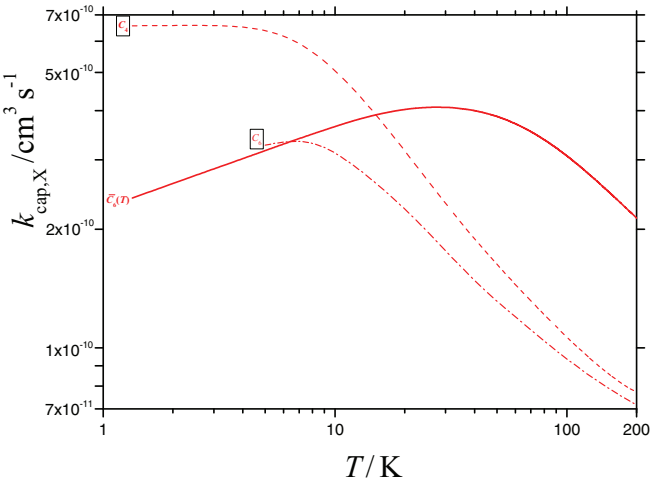

FIG. 6. Thermal rate constants for capture into the ground electronic state of the adduct COH($\mathrm{X}^2\mathrm{A}'$) (—, red: $k^{\mathrm{NBO}}_{\mathrm{cap,X}}$, as in Fig. 5; —-, red dashed: $k^{\mathrm{BO}}_{\mathrm{cap,X}}$, see Sec. IV; - · - · -, red dashed-dotted: single SBO – CT calculations $k^{\mathrm{BO,CT}}_{\mathrm{cap,X}}$ of Ref. 16; $\bar{C}_6(T)$, $\boxed{C_4}$, and $\boxed{C_6}$ mark the low-temperature limits of Eqs. (4.7), (4.10), and (4.11), respectively).

at higher temperatures. Therefore, with $\bar{C}_6(T)$ from Eq. (3.6), Eq. (4.6) in the intermediate temperature range is replaced by

$$k^{\mathrm{NBO}}_{\mathrm{cap,X}}(T \to 0\,\mathrm{K}) \to 2.43 \times 10^{-10}(T/\mathrm{K})^{1/6}\,\mathrm{cm}^3\mathrm{s}^{-1}. \tag{4.7}$$

This value in turn is close to the CT results from Ref. 27 which corresponded to nearly the same effective value of C_6, see below.

We briefly also consider the role of the few narrowly avoided crossings which originate from the Λ – coupling within groups of channels with given good quantum number P (see Sec. II). An assumption that all narrowly avoided crossings with a splitting smaller than 0.1 B are passed diabatically leads to only minimal changes in the SACM capture rate constant (indicated by the dashed line in Fig. 5). This is the result of only negligible changes in the branching into electronic states of the adduct. For example, only one doubly degenerate channel with $|P| = 1/2$ changes its branching and leads from the lowest rotronic state with $J_{\mathrm{C}} = 1$ into the excited electronic state of the adduct, $1^2\mathrm{A}''$; vice versa, assuming complete channel adiabaticity, all such channels starting with $J_{\mathrm{C}} = 1$ lead into the ground electronic state $\mathrm{X}^2\mathrm{A}'$ (as shown in Figs. 2–4). We emphasize again that the AC specification of the electronic state only holds for the initial approach of the reactants until the chosen distance of 5 a.u. is reached; electronically nonadiabatic and intramolecular vibrational transitions are likely to occur later on, but are not considered in the present analysis.

As we were able to specify NBO ACs with respect to the attained electronic state (at distances of about 5 a.u.), we also calculated thermal rate constants for capture into specific electronic states. In this case Q^* analogous to Eq. (4.3) was determined for ACs ending in such electronic states. Fig. 5 includes results for formation of adducts in the states $\mathrm{X}^2\mathrm{A}'$, $1^2\mathrm{A}''$, $1^4\mathrm{A}'$, and$1^4\mathrm{A}''$; the total rate constant $k^{\mathrm{NBO}}_{\mathrm{cap}}(T)$ for capture in all of these states is also given (capture into 8 higher excited electronic states of the adduct here is neglected). Capture into the excited states $1^2\mathrm{A}''$, $1^4\mathrm{A}'$, and $1^4\mathrm{A}''$ shows a threshold behavior; capture into $1^2\mathrm{A}''$ and $1^4\mathrm{A}''$ prevails over capture into $1^4\mathrm{A}'$. The total capture rate constant $k^{\mathrm{NBO}}_{\mathrm{cap}}(T)$ has a rather flat temperature dependence with a not very pronounced maximum near to 70 K.

The comparison of the derived $k^{\mathrm{NBO}}_{\mathrm{cap,X}}(T)$ with the corresponding $k^{\mathrm{BO}}_{\mathrm{cap,X}}(T)$ from the conventional SACM treatment corrected using Eq. (1.1) shows marked differences such as illustrated in Fig. 6. In SACM calculations, $Q^{*\mathrm{BO}}_{\mathrm{X}}$ includes contributions from hindered rotor ACs as calculated with the asymptotic PES of $\mathrm{X}^2\mathrm{A}'$ neglecting SO-coupling (see Sec. III). The corresponding Q is equal to the rotational partition function (the electronic degeneracy of the doublet state cancels here)

$$Q^{\mathrm{rot}}(T) = \sum_{J_{\mathrm{rot}} \geq 0} (2J_{\mathrm{rot}} + 1)\exp\left[-J_{\mathrm{rot}}(J_{\mathrm{rot}} + 1)\,B/k_{\mathrm{B}}T\right]. \tag{4.8}$$

The electronic factor $f_{\mathrm{el}}(T)$ in this case accounts for the thermal population of the lowest electronic state of the reactants which a assumed to contribute exclusively to $k^{\mathrm{BO}}_{\mathrm{cap,X}}(T)$, and it

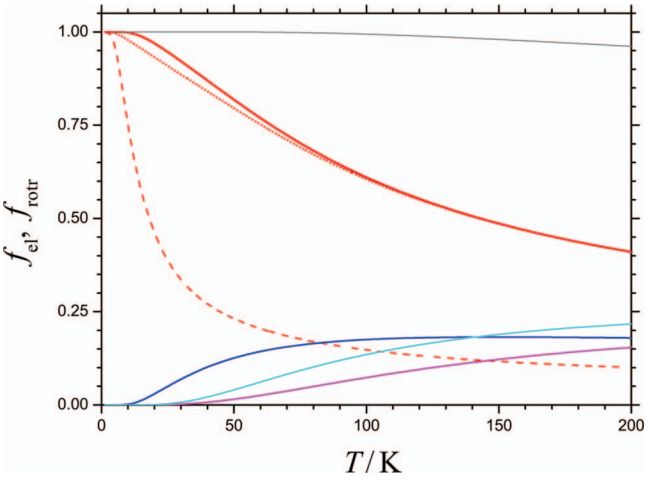

FIG. 7. Thermal branching factors f_{el} and f_{rotr} (—, red dashed: f_{el} from Eq. (4.9); —, red: f_{rotr} from Eq. (4.12) for branching into X^2A' with adiabatic, or diabatic (· · · · , dotted red), passage through narrowly avoided crossings, see Sec. IV; —, blue; —, pink; and —, cyan: f_{rotr} for branching (adiabatic passage) into the $1^2A''$, $1^4A'$, and $1^4A''$ electronic states of the adduct, respectively; —, gray: f_{rotr} for branching into the four lowest electronic states of the adduct).

is given by

$$f_{el}(T) = \{1 + \exp[-A/k_B T]\}^{-1}\{1 + 3\exp[-2a/k_B T] + 5\exp[-6a/k_B T]\}^{-1}. \quad (4.9)$$

f_{el} and Q^{rot} approach unity at $T \to 0$ K. Q_X^{*NBO}, on the other hand, at low temperatures is calculated with the AC potential of Eq. (3.2) as given by $V(R) = -C_4 R^{-4}$. With this R – dependence the limiting low temperature capture rate constant becomes temperature independent (analogous to the Langevin rate constant for ion-induced dipole capture). One obtains Langevin type (see $\boxed{C_4}$ in Fig. 7) and is given by

$$f_{el}(T = 0\,\text{K}) = 1, \quad Q^{rot}(T = 0\,\text{K}) = 1, \quad (4.10)$$

$$k_{cap,X}^{BO}(T \to 0\,\text{K}) = 2\pi\sqrt{\frac{3d\langle r_C^2\rangle}{10\mu}\left(3 + \frac{1}{\sqrt{5}}\ln\left[\frac{47 + 21\sqrt{5}}{2}\right]\right)} = 6.4 \times 10^{-10}\,\text{cm}^3\text{s}^{-1}.$$

See the curve labeled $\boxed{C_4}$ in Fig. 6. Due to the $T^{1/6}$ – dependence of k_{cap} in Eqs. (4.5) and (4.6), the capture rate constant from the NBO calculations at $T < 15$ K becomes smaller than th BO values from Eq. (4.10). At higher temperatures, on the other hand, $k_{cap,X}^{BO}(T)$ falls markedly below $k_{cap,X}^{NBO}(T)$ which is mostly due to the rapid decrease of $f_{el}(T)$ (and finally due to the BO assumption that only the lowest electronic state of the free reactants participates in $k_{cap,X}^{BO}(T)$). One should note that $k_{cap,X}^{BO}(T)/f_{el}(T)$ exceeds the total capture rate constant $k_{cap}^{NBO}(T)$ at all temperatures, partly because the excited electronic states of the reactants are less attractive and thus less effective in capture as their ground electronic state.

We next compare the present calculations of $k_{cap,X}^{NBO}(T)$ and $k_{cap,X}^{BO}(T)$ with the results from the CT calculations $k_{cap,X}^{BO,CT}(T)$ of Ref. 27. Fig. 6 illustrates this comparison. We first note a difference between $k_{cap,X}^{BO,CT}(T)$ and $k_{cap,X}^{BO}(T)$ at the lowest temperatures where the electronic factor, f_{el}, being contained in both quantities, approaches unity. This difference is due to the difference in the long-range asymptotic behavior of the used PES for the X^2A' electronic state. The CT calculations of Ref. 27, unlike our asymptotic theory, employ the *ab initio* PES from Ref. 26 and the isotropic potential $-C_6R^{-6}$ as its asymptotic continuation. With the corresponding $C_6 = 97.3$ a.u., see above, the low-temperature semi-classical rate constant (see curve $\boxed{C_6}$ in Fig. 6) then approaches

$$k_{cap,X}^{BO,CT}(T \to 0\,\text{K}) \to 2^{11/6}\Gamma(2/3)\sqrt{\pi/\mu}C_6^{1/3}T^{1/6} = 2.6 \times 10^{-10}(T/\text{K})^{1/6}\,\text{cm}^3\text{s}^{-1}. \quad (4.11)$$

The comparison with Eq. (4.7) shows that this choice of the asymptotic potential in the CT calculations accidentally reproduces the low temperature effect of SO-coupling (which actually was neglected in the employed *ab initio* PES of Ref. 26). $k_{cap,X}^{BO,CT}(T)$ and $k_{cap,X}^{BO}(T)$ approach each other at higher temperatures when the differences in the asymptotic behavior of the PES loose importance and the similar intermediate part of the *ab initio* PES matters most. As it was repeatedly noted (see, e.g., Refs. 8–12), SACM and CT for the same PES approach each other at temperatures with $k_B T > B$.

It was stated before that the drop of $f_{el}(T)$ with increasing temperature is the main factor responsible for the decline of $k_{cap,X}^{BO}(T)$. Having described the branching of the free reactant states into the different electronic states of the adduct in Sec. III (see Figs. 2–4), one may also define a rotronic thermal branching factors $f_{rotr}(T)$ analogous to $f_{el}(T)$, now specifying the fraction of the free reactant rotronic state population which in the NBO approach leads into the electronic ground state. This $f_{rotr}(T)$ then is defined by

$$f_{rotr}(T) = Q_X^{rotr}(T)/Q^{rotr}(T), \quad Q_X^{rotr}(T) = \sum_i g_i^X \exp[-E_i/k_B T], \quad (4.12)$$

where $Q_X^{rotr}(T)$ includes the entrance states branching into X^2A'. Because of complete branching into X^2A' from the ground rotronic state of the free reactants, the factor $f_{rotr}(T)$ as well as the factor $f_{el}(T)$ approach unity for $T \to 0$ K. However, $f_{rotr}(T)$ decreases much more slowly with T than $f_{el}(T)$. Fig. 7 illustrates this difference. It is the consequence of the differences in the branching such as illustrated in Fig. 4. For example, the lowest rotronic states with $J_C \neq 0$ in the NBO approach lead into the ground state of the adduct, whereas the corresponding excited electronic states of the free reactants do not correlate adiabatically with X^2A' and, as a consequence, do not contribute to capture into this state in the BO approximation. Fig. 7 includes also rotronic factors for NBO branching into excited electronic states of the adduct. In the presented temperature range, the shown rotronic factors from the NBO approach nearly sum up to unity (the small drop to 0.95 at 200 K is due to the omission of 8 upper excited electronic states of the adduct which start to contribute at higher

temperatures). It should be mentioned again that switching to the assumption that all narrowly avoided crossings with a splitting smaller than 0.1 B are passed diabatically, leads only to minimal changes in the $f_{\rm rotr}(T)$ (see the dotted line in Fig. 7).

V. CONCLUSIONS

The present work provided a statistical adiabatic channel treatment of the formation of adducts at low temperature by capture in collisions between two open electronic shell species. The capture in collisions between $C(^3P)$ and $OH(^2\Pi)$ was used as a representative example. Adiabatic channel potential curves were obtained by direct diagonalization of the rotronic Hamiltonian containing asymptotic interactions. Along with the long-range electrostatic multipole, induction, and dispersion interactions, also exchange interaction and spin–orbit coupling were taken into account. By exploiting explicit correlation rules for the projection of angular momenta onto the interreactant axis (corresponding to good quantum numbers within various approximations) and employing a suitable matching procedure at intermediate interreactant distances, the individual adiabatic channels could be specified with respect to the electronic states reached in adduct formation.

A series of details of the procedure and results deserve particular mention. By slightly adjusting the pre-exponential factors of the asymptotic single-center atomic/molecular orbitals used for the construction of the exchange interaction (see Eq. (2.13)), the *ab initio* PESs of the C + OH system from Refs. 26 and 29 at intermediate distances could be almost quantitatively reproduced. Including spin–orbit coupling, the asymptotic PESs indicated a multitude of areas with electronic nonadiabaticity. This nonadiabaticity mainly is responsible for the fact that our calculated capture rate constants at the considered temperatures (up to 200 K) markedly exceed the results obtained by CT calculations on the single electronic ground state PES corrected by the statistical electronic factor $f_{\rm el}(T)$ (Ref. 16). The maximum of the rate constant in our results is shifted from about 7 (Ref. 27) to 30 K and the decrease with increasing temperature beyond the maximum is much less pronounced.

The present result of the inadequacy of Eq. (1.1) is probably general and it is of considerable practical importance for rate constants of capture-controlled radical–radical reactions at temperatures below room temperature. As measurements in this range often are difficult and results sometimes are controversial, calculations of the present type can help to improve the situation. Except for particularly low temperatures, the present approach will mostly lead to rate constants which are higher than obtained with Eq. (1.1). The reason for the differences between the present NBO and conventional single BO treatments (SACM or CT) are easily traced. There is, first, the marked difference between the conventional electronic factor $f_{\rm el}(T)$ and its analog, the rotronic factor $f_{\rm rotr}(T)$, see Sec. IV. A much larger number of adiabatic channels in the NBO approach correlate with the electronic ground state of the adduct than in the BO treatment (e.g., in the NBO approach the lowest rotronic states arising from $C(^3P_1)$, in contrast to the conventional BO treatment, lead into the ground electronic state of the adduct). Second, the overall capture rate constant for capture into any of the electronic states of the adduct in the NBO approach is smaller than the corresponding BO rate constant, see Fig. 5. In the language of the BO treatment one might explain this by the more attractive lowest SBO potential in comparison to an effective overall potential in the NBO treatment. The effect of adiabatic vs diabatic dynamics at the few narrowly avoided crossings of the channel potentials was shown to be unimportant at the considered temperatures. On the whole, the difference between the factors $f_{\rm el}(T)$ and $f_{\rm rotr}(T)$ obviously is the dominant reason for the marked difference between $k^{\rm BO}_{\rm cap,X}(T)$ and $k^{\rm NBO}_{\rm cap,X}(T)$.

ACKNOWLEDGMENTS

Helpful discussions with V. G. Ushakov are gratefully acknowledged. We are also grateful for critical reading of the manuscript and helpful suggestions by B. Bussery-Honvault and M. H. Alexander.

APPENDIX: INTERREACTANT SYSTEM, ASYMPTOTIC INTERACTIONS, PESs, AND ASYMPTOTIC ADIABATIC CHANNEL POTENTIALS

1. Frames and momentum projections

Space-fixed frame. z-axis: along the interreactant axis **R** (from center of mass of OH to C), x-axis: along the reactant orbital momentum ℓ; Euler angles for transformation to the body-fixed (molecular) frame: φ, θ, χ.

Body-fixed (molecular) frame. ζ-axis along the molecular axis **r** (from O to H), ξ-axis in and η-axis orthogonal to the plane of the atom–diatom system; polar and azimuthal angular coordinates with respect to ζ-axis: ϑ, ϕ.

TABLE I. Projections of momenta onto the axis of the body- and space-fixed frames.

Projections onto the axis of the body-fixed frame:		
Λ	of total rotronic (NSO) momentum K of OH	onto ζ-axis
Ω	of total rotronic momentum $J_{\rm OH}$	onto ζ-axis
Projections onto the axis of the space-fixed frame:		
ℓ	of total momentum J of the system ($\ell \approx J$)	onto x-axis
M_L	of electronic (NSO) momentum $L = 1$ of C	onto z-axis
M_{J_C}	of total spin electronic momentum J_C of C	onto z-axis
M_S	of total spin (NSO) momentum S of the system	onto z-axis
M_K	of total rotronic (NSO) momentum K of OH	onto z-axis
$N = M_L + M_K$	of total rotronic (NSO) momentum of the system	onto z-axis
$P = N + M_S$	of total rotronic momentum of the system	onto z-axis
M	of rotational momentum $J_{\rm rot}$ of linear rotor OH	onto z-axis

2. Long-range interaction terms $U^{lr}(R)$ for C + OH

The electronic functions of C($2p^2$, ^{3}P) are given by

$$\begin{aligned}
\langle L=1, M_L=1| &= -\left\{C^{11}_{11,10}Y_{11}(1)\,Y_{10}(2)\right.\\
&\left.+\,C^{11}_{10,11}Y_{10}(1)\,Y_{11}(2)\right\}R_{21},\\
\langle L=1, M_L=0| &= \left\{C^{10}_{11,1-1}Y_{11}(1)\,Y_{1-1}(2)\right.\\
&\left.+\,C^{10}_{1-1,11}Y_{1-1}(1)\,Y_{11}(2)\right\}R_{20},\\
\langle L=1, M_L=-1| &= \left\{C^{1-1}_{1-1,10}Y_{1-1}(1)\,Y_{10}(2)\right.\\
&\left.+\,C^{1-1}_{10,1-1}Y_{10}(1)\,Y_{1-1}(2)\right\}R_{21}
\end{aligned} \tag{A1}$$

(see Ref. 52) where the $R_{2\,M_L}$ are products of two one-electron radial p-wave functions, and the $Y_{1m}(i) = Y_{1m}(\vartheta_i, \phi_i)$ are one-electron spherical harmonics with polar, ϑ_i, and azimuthal, ϕ_i, electronic spherical coordinates (referred to the interreactant axis z and the azimuthal $\xi\zeta$-plane of the adduct including this axis, see Subsection A 1 of the Appendix). Upon reflection of the electronic coordinates in the $\xi\zeta$-plane, the functions in Eq. (A1) transform as

$$\langle L=1, M_L| \rightarrow (-1)^{M_L}\,\langle L=1, -M_L|. \tag{A2}$$

The phase factor $(-1)^{M_L(M_L+1)/2}$ included in Eq. (A1) guarantees the standard form of the transformation of Eq. (A2) (see, e.g., Ref. 48).

The multipole expansion of the electrostatic interaction up to R^{-6} terms corresponds to the interaction of the quadrupole moment of C(^{3}P) with the dipole, quadrupole, and octupole moments of OH($^2\Pi$). The matrix elements of the quadrupole moment of C($2p^2$, ^{3}P) are expressed as

$$\begin{aligned}
&\left\langle L=1, M'_L\right| Q^{(C)}_{2\,m}\left|L=1, M_L\right\rangle\\
&\quad=(-1)^{\left(M_L+{M_L}^2+M'_L+{M'_L}^2\right)/2}\left(C^{1\,M'_L}_{1\,M_L,2\,m}/C^{1\,0}_{1\,0,2\,0}\right)Q^{(C)}_0,\\
&Q^{(C)}_0=-2\left\langle Y_{11}\right|P_2\left|Y_{11}\right\rangle\left\langle r^2_C\right\rangle=-2\left\langle r^2_C\right\rangle/5,
\end{aligned} \tag{A3}$$

where $\langle r^2_C\rangle = 3.89$[50] corresponds to the square of the electronic radius averaged over the radial p-wave function. The matrix elements of the multipole moments of OH($^2\Pi$) are calculated using molecular orbitals from Ref. 53 (except for the dipole moment for which its experimental value of 0.651 is taken from Ref. 54). Table II lists the matrix elements of the electrostatic moments of OH which are used as reference values. These are defined as[55]

$$\begin{aligned}
&q^+_{lm}=\langle x|\,Q^+_{lm}\,|x\rangle\,,\ m\geq 0,\\
&\langle x|=\left(\langle\Lambda=1|-\langle\Lambda=-1|\right)/\sqrt{2},\\
&Q^p_{lm}=i^{(1-p)/2}\left\{p\,(-1)^m\,Q_{lm}+Q_{l-m}\right\}/\sqrt{2\left(1+\delta_{m,0}\right)},\ p=\pm1
\end{aligned} \tag{A4}$$

TABLE II. Reference matrix elements of the multipole electrostatic moments of OH.

l	m	q^+_{lm}
1	0	0.702
2	0	1.202
2	2	−0.738
3	0	2.175
3	2	0.044

and can be converted into the matrix elements of the multipole moments of OH by

$$\begin{aligned}
\langle 1|\,Q_{1\,0}\,|1\rangle &= \langle -1|\,Q_{1\,0}\,|-1\rangle = q^+_{1\,0}=d,\\
\langle 1|\,Q_{l\,0}\,|1\rangle &= \langle -1|\,Q_{l\,0}\,|-1\rangle = q^+_{l\,0},\ l=2,3,\\
\langle 1|\,Q_{l\,-2}\,|-1\rangle &= \langle -1|\,Q_{l\,2}\,|1\rangle = c\,q^+_{l\,2},\ l=2,3,
\end{aligned} \tag{A5}$$

$$\begin{aligned}
c^{-1} &= \frac{1}{2\pi}\int_0^{2\pi}\frac{Y^2_l(\phi)+Y^{-2}_l(\phi)}{\sqrt{2}Y^2_l(0)}\\
&\quad\times\left[\frac{Y^1_1(\phi)-Y^{-1}_1(\phi)}{\sqrt{2}Y^1_1(0)}\right]^2\mathrm{d}\phi\\
&=\left(2\sqrt{2}/2\pi\right)\int_0^{2\pi}\cos 2\phi\cos^2\phi\;\mathrm{d}\phi=1/\sqrt{2},
\end{aligned}$$

where the integration variable ϕ is the azimuthal angle of the orientation of the multipole moment relative to the axis of OH (the specification of the polar angle variable in the spherical harmonics here is omitted).

The matrix representation of U^{elst} (see, e.g., Ref. 28) in the basis of the functions of Eq. (2.9) is given by

$$\begin{aligned}
&\left\langle L, M'_L, S', M'_S, \Lambda'\right|U^{\mathrm{elst}}\left|L, M_L, S, M_S, \Lambda\right\rangle\\
&\quad=\delta_{S',S}\delta_{M'_S,M_S}\sum_{l=1,2,3}(-1)^l\,R^{-l-3}\sqrt{\binom{2l+4}{4}}\\
&\quad\times\sum_m C^{l+2\,0}_{2m,l-m}\left\langle L=1, M'\right|Q^{(C)}_{2\,m}\left|L=1, M_L\right\rangle\\
&\quad\times\langle\Lambda'|Q_{l\,\Lambda'-\Lambda}\,|\Lambda\rangle\,d^l_{-m,\Lambda'-\Lambda}(\theta)\,,
\end{aligned} \tag{A6}$$

where $d^l_{-m,\Lambda'-\Lambda}(\theta)$ is the Wigner function of the polar angle θ.

In the linear configurations of the system OHC/COH (θ = 0 or π, respectively), the main contributions come from the dipole–quadrupole ($\propto R^{-4}$) and quadrupole–quadrupole ($\propto R^{-5}$) terms which determine the energetic sequence of the electronic states. (The corresponding terms are given in Table S.1 of the supplementary material.[60]) In the T-shaped configuration ($\theta = \pi/2$), the energetic sequence of the six, spin-degenerate (SO interaction neglected), electronic states consists of 3 groups which are split due to the axial symmetry of the quadrupole-quadrupole interaction into lower A′ and upper A″ subcomponents. (The corresponding terms are given

in Table S.2 of the supplementary material.[60]) We note full agreement with the results of Ref. 28.

The induction ($U^{\rm ind}$) and dispersion ($U^{\rm disp}$) terms are proportional to $R^{-6}$and originate from the static and dynamical anisotropic dipole polarizabilities of the reactants.[28,55] Repeating the procedure of Ref. 28, we calculated state- and anisotropy-specific coefficients ${}^{\rm ind}V_{6,\,L_bM_aM_b}^{M_LM'_L,\Lambda\Lambda'}$ and ${}^{\rm disp}V_{6,\,L_bM_aM_b}^{M_LM'_L,\Lambda\Lambda'}$ of the expansion of the matrix elements of $U^{\rm ind}$ and $U^{\rm disp}$, respectively,

$$\begin{aligned}\left\langle L,\,M_L,\,S,\,M_S,\,\Lambda\right|U^{\rm ind}+U^{\rm disp}\left|L,\,M'_L,\,S',\,M'_S,\,\Lambda'\right\rangle \\ =-R^{-6}\delta_{S,S'}\delta_{M_SM'_S}\sum_{L_b,M_a,M_b} \\ \times\left({}^{\rm ind}V_{6,\,L_bM_aM_b}^{M_LM'_L,\Lambda\Lambda'}+{}^{\rm disp}V_{6,\,L_bM_aM_b}^{M_LM'_L,\Lambda\Lambda'}\right)d^{L_b}_{-M_a,M_b}(\theta)\,.\end{aligned} \tag{A7}$$

The results were in agreement with Ref. 28. They are shown in Table III. Octupole–quadrupole, induction, and dispersion interactions in first order lead to additional contributions to the PESs in the form $A_6(\theta)/R^6$. In the linear configurations ($\theta = 0$ and π), there are no other than these additional contributions $\propto R^{-6}$. In the T-shaped configuration, the contributions $A_6(\pi/2)/R^6$ to the asymptotic PESs consist both of first order octupole–quadrupole, induction, and dispersion terms as well as of second order terms from the quadrupole–quadrupole interaction. (These terms are given in Table S.4 of the supplementary material.[60])

TABLE III. State- and anisotropy-specific coefficients for induction and dispersion terms in Eq. (A7), bold type – from this work, in parentheses – from Ref. 28.

m_L	m'_L	$\Lambda,\,\Lambda'$	L_b	M_a	M_b	${}^{\rm ind}V_{6,\,L_bM_aM_b}^{M_LM'_L,\Lambda\Lambda'}$
−1	−1	±1, ±1	0	0	0	**5.081** (5.106)
−1	−1	±1, ±1	2	0	0	**5.368** (5.407)
−1	0	±1, ±1	2	−1	0	**−0.498** (−0.522)
−1	1	±1, ±1	2	−2	0	**0.352** (0.369)
0	−1	±1, ±1	2	1	0	**0.498** (0.522)
0	0	±1, ±1	0	0	0	**4.650** (4.654)
0	0	±1, ±1	2	0	0	**4.075** (4.051)
m_L	m'_L	$\Lambda,\,\Lambda'$	L_b	M_a	M_b	${}^{\rm disp}V_{6,\,L_bM_aM_b}^{M_LM'_L,\Lambda\Lambda'}$
±1	±1	±1, ±1	0	0	0	**36.357** (36.529)
±1	±1	±1, ±1	2	0	0	**2.859** (2.871)
±1	0	±1, ±1	2	±1	0	**±0.164** (−0.168)
±1	∓1	±1, ±1	2	±2	0	**−0.116** (0.119)*
0	±1	±1, ±1	2	∓1	0	**∓0.164** (0.168)
0	0	±1, ±1	0	0	0	**34.609** (34.737)
0	0	±1, ±1	2	0	0	**2.432** (2.435)
±1	±1	±1, ∓1	2	0	±2	**−1.523** (1.532)*
±1	0	±1, ∓1	2	±1	±2	**∓0.106**(−0.109)
±1	∓1	±1, ∓1	2	±2	±2	**0.075** (0.077)
0	±1	±1, ∓1	2	∓1	±2	**±0.106** (0.109)
0	0	±1, ∓1	2	0	±2	**−1.247** (1.248)*

TABLE IV. Parameters of the asymptotic orbital wave functions of Eq. (2.13)

q	Orbital	γ_q	A_q
1	C,2p	0.9097	1.6
2	OH,1π	0.9775	1.6
3	C,2s	1.1043	2.0
4	OH,3σ	1.1012	2.0

3. Asymptotic exchange interaction terms $U^{\rm ex}$ for C + OH

In the linear configurations of the system, OHC or COH, the contributions from the exponentially small exchange interaction can be expressed through the exchange integral functions. Table S.5 of the supplemental material[60] shows the corresponding contributions which are symmetric with respect to the transformation $\theta \to \pi - \theta$ (the sum $\gamma_q + \gamma_{q'}$ of parameters from Eq. (2.13) here is replaced by $\mu_{(q,\,q')}$). One notices that mainly the exchange interactions with the inner orbital of OH ($q' = 4$) contribute to the repulsion in the linear configurations (we focus here on the contributions from the leading exchange integral functions with $k = n = 0$).

In the T-shaped configuration of the system at large R, the transformation to the diagonal form of the leading dipole-quadrupole component of $U^{\rm lr}$ (see Eq. (2.12)) also allows one to estimate the additional, exponentially small, first order contributions of $U^{\rm ex}$. (This is illustrated in the lines (a) of Table S.6 of the supplemental material.[60]) In the table only the terms including the leading exchange integral functions with $k = n = 0$ are retained, while the main contribution from $U^{\rm lr}$ to the PESs here can be extracted from Table S.2 of the supplementary material.[60] The additional attraction in this configuration is due to the exchange interaction of the outer shells

TABLE V. Fitting coefficients for the exchange integral functions (see Eq. (2.15)).

q	q'	k	n	$100a_{kn}^{(q,q')}$	$10b_{kn}^{(q,q')}$	$c_{kn}^{(q,q')}$	$d_{kn}^{(q,q')}$
1	2	0	0	0.1690	−0.5275	−1.1452	1.2501
1	2	1	0	0.1690	−0.5275	−1.1456	0.6145
1	2	1	1	0.1690	−0.5284	−1.1175	1.187
1	2	1	−1	0.1692	−0.5283	−1.1735	1.1071
1	2	2	0	0.1690	−0.5275	−1.1461	−0.0209
1	4	0	0	0.1461	−0.4352	−1.3471	1.6914
1	4	1	0	0.1462	−0.4348	−1.3504	0.9898
1	4	1	1	0.1459	−0.4463	−1.2658	1.6444
1	4	1	−1	0.1512	−0.4405	−1.4316	1.4493
1	4	2	0	0.1463	−0.4346	−1.3538	0.2899
3	2	0	0	0.1349	−0.4116	−1.4835	1.7033
3	2	1	−1	0.1345	−0.4157	−1.4288	1.6005
3	4	0	0	0.1157	−0.3639	−1.6985	2.1608
3	4	1	−1	0.1157	−0.3639	−1.6971	1.9666
1	4	2	0	0.1463	−0.4346	−1.3538	0.2899
3	2	0	0	0.1349	−0.4116	−1.4835	1.7033
3	2	1	−1	0.1345	−0.4157	−1.4288	1.6005
3	4	0	0	0.1157	−0.3639	−1.6985	2.1608
3	4	1	−1	0.1157	−0.3639	−1.6971	1.9666

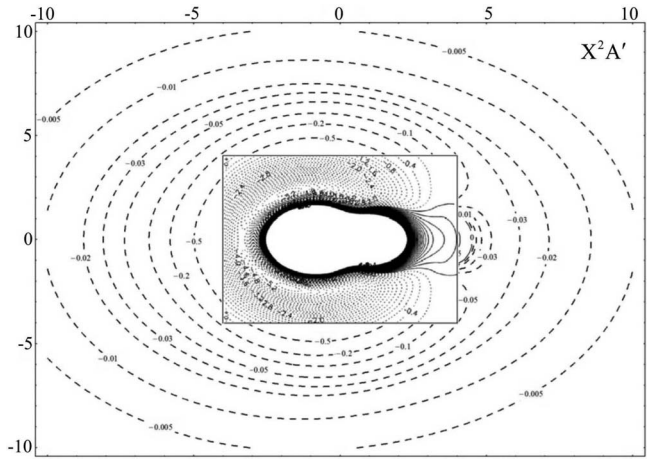

FIG. 8. Contour plots of the PES of the lowest electronic state (X^2A') of COH (calculations without SO-coupling; coordinates as in Fig. 1; energies in eV; outer part from this work, inner part from the *ab initio* calculations of Refs. 26 and 29), see text in Sec. II B.

($q = 1$, $q' = 2$), being maximal in the $2^2A'$ state. In the ground state X^2A' at large R this interaction even produces a repulsive contribution, see Table S.6 of the supplementary material.[60] Because we could not make an analytical predic-

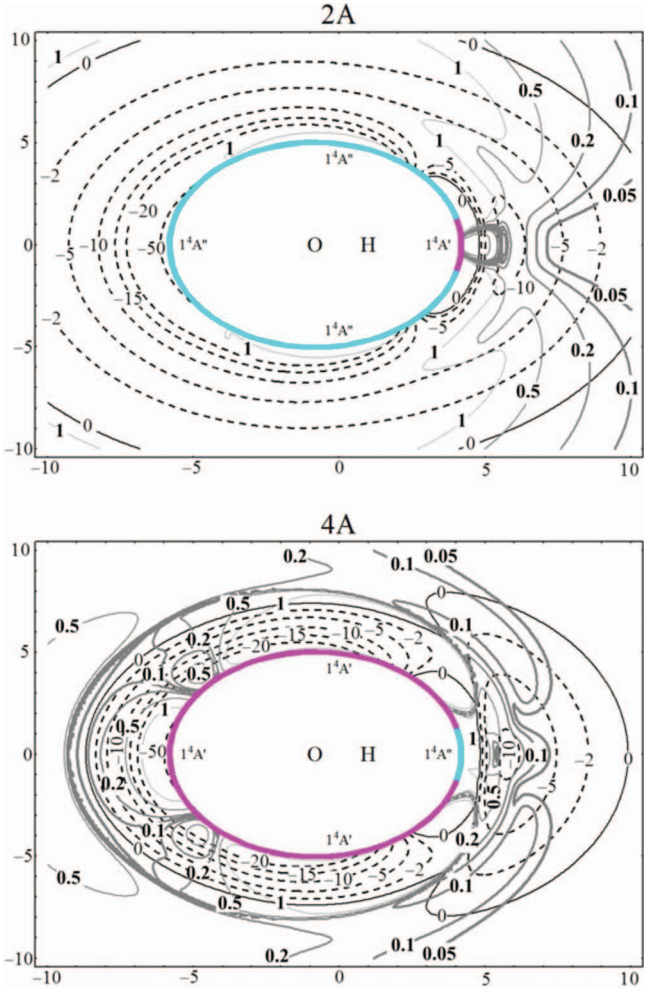

FIG. 9. As Fig. 1, for higher electronic states of the adduct, see text in Sec. II B.

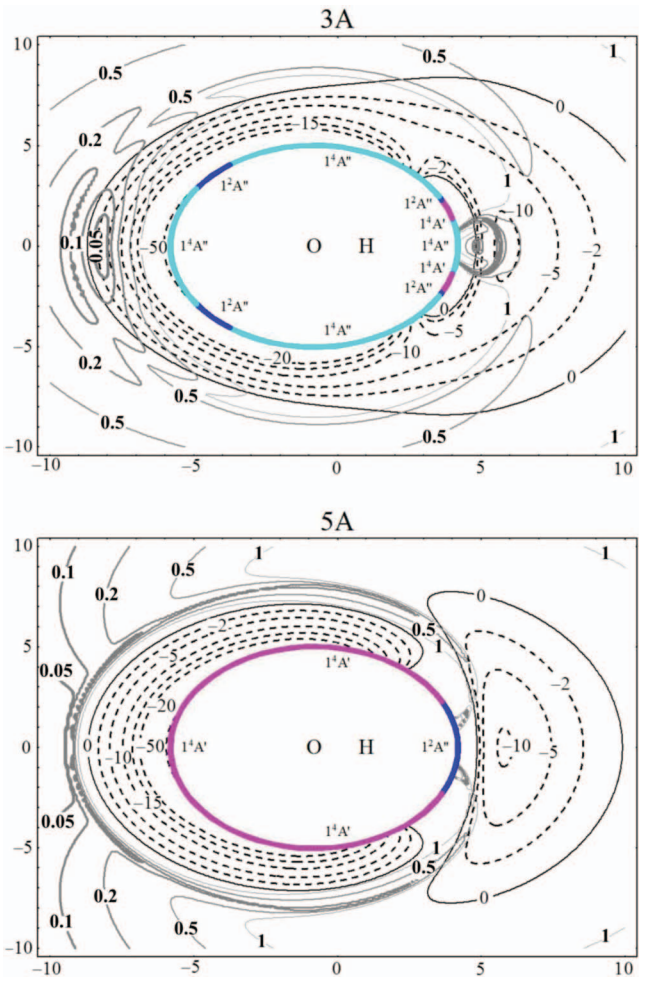

FIG. 10. As Fig. 1, for higher electronic states of the adduct, see text in Sec. II B.

tion for the T-shaped configuration in a situation of comparable long-range and short-range exchange contributions, here we designed a hypothetical model. In this model the exchange interactions prevailed and non-exchange contributions were neglected. We kept again the leading exchange integral functions only. The results are given in the lines (m) of Table S.6 of the supplementary material.[60] For the T-shaped configuration this model showed maximal attraction in 1^2A states. Nevertheless, it made no difference between the PES components of different reflection symmetry. In order to sort these states by their energy, one has also to consider the exchange integral functions with n or k different from zero and to take

TABLE VI. Leading terms of the lowest adiabatic channel potentials ($K = 1$) in the NBO(NSO) approximation.

$\|N\|$	$V_{\|N\|}(R) - B$
2	$-\frac{3d\langle r_C^2\rangle}{10R^4}$, $\frac{3d\langle r_C^2\rangle}{10R^4}$
1	$-\frac{3(\sqrt{2}+1)d\langle r_C^2\rangle}{10R^4}$, $-\frac{3(\sqrt{2}-1)d\langle r_C^2\rangle}{10R^4}$, $\frac{3(\sqrt{2}-1)d\langle r_C^2\rangle}{10R^4}$, $\frac{3(\sqrt{2}+1)d\langle r_C^2\rangle}{10R^4}$
0	$-\frac{3\sqrt{3}d\langle r_C^2\rangle}{10R^4}$, $-\frac{3\sqrt{3}d\langle r_C^2\rangle}{10R^4}$, 0, 0, $\frac{3\sqrt{3}d\langle r_C^2\rangle}{10R^4}$, $\left(\frac{3\sqrt{3}d\langle r_C^2\rangle}{10R^4}\right)$

TABLE VII. R^{-6} and R^{-8} coefficients of AC potentials used in Eqs. (3.4) and (3.5).

$$
\begin{aligned}
{}^6V_{|P|=\frac{3}{2}} &= -R^{-6}\left(\tfrac{2}{3}{}^{\mathrm{ind}}V^{-1\,-1,-1\,-1}_{6,000} + \tfrac{1}{3}{}^{\mathrm{ind}}V^{00,-1\,-1}_{6,000} + \tfrac{2}{15}{}^{\mathrm{ind}}V^{-1\,-1,-1\,-1}_{6,200} + \tfrac{1}{15}{}^{\mathrm{ind}}V^{00,-1\,-1}_{6,200} + \right.\\
&\quad \left. + \tfrac{2}{3}{}^{\mathrm{disp}}V^{-1\,-1,-1\,-1}_{6,000} + \tfrac{1}{3}{}^{\mathrm{disp}}V^{00,-1\,-1}_{6,000} + \tfrac{2}{15}{}^{\mathrm{disp}}V^{-1\,-1,-1\,-1}_{6,200} + \tfrac{1}{15}{}^{\mathrm{disp}}V^{00,-1\,-1}_{6,200}\right),\\
{}^6V_{|P|=\frac{1}{2}} &= -R^{-6}\left(\tfrac{2}{3}{}^{\mathrm{ind}}V^{-1\,-1,-1\,-1}_{6,000} + \tfrac{1}{3}{}^{\mathrm{ind}}V^{00,-1\,-1}_{6,000} - \tfrac{2}{15}{}^{\mathrm{ind}}V^{-1\,-1,-1\,-1}_{6,200} - \tfrac{1}{15}{}^{\mathrm{ind}}V^{00,-1\,-1}_{6,200} + \right.\\
&\quad \left. + \tfrac{2}{3}{}^{\mathrm{disp}}V^{-1\,-1,-1\,-1}_{6,000} + \tfrac{1}{3}{}^{\mathrm{disp}}V^{00,-1\,-1}_{6,000} - \tfrac{2}{15}{}^{\mathrm{disp}}V^{-1\,-1,-1\,-1}_{6,200} - \tfrac{1}{15}{}^{\mathrm{disp}}V^{00,-1\,-1}_{6,200}\right)
\end{aligned}
$$

$$
\begin{aligned}
{}^8V_{|P|=\frac{3}{2}} &= -\frac{6d^2\langle r_C\rangle^2}{25R^8}\left\{\frac{\left[C^{3/2\,-3/2}_{3/2\,-3/2,1\,0}\right]^2\left(\left[C^{3/2\,1/2}_{3/2\,3/2,1\,-1}\right]^2+3\left[C^{3/2\,3/2}_{3/2\,3/2,1\,0}\right]^2\right)}{6a}\right.\\
&\quad \left. + \frac{2\left[C^{5/2\,-3/2}_{3/2\,-3/2,1\,0}\right]^2\left(\left[C^{5/2\,1/2}_{3/2\,3/2,1\,-1}\right]^2+3\left[C^{5/2\,3/2}_{3/2\,3/2,1\,0}\right]^2\right)}{3(6a+5B)}\right\}\\
&= -\frac{d^2\langle r_C\rangle^2}{625R^8}\left(\frac{198}{6a}+\frac{52}{6a+5B}\right),\\
{}^8V_{|P|=\frac{1}{2}} &= -\frac{6d^2\langle r_C\rangle^2}{25R^8}\left\{\frac{\left[C^{3/2\,-3/2}_{3/2\,-3/2,1\,0}\right]^2\left(\left[C^{3/2\,-3/2}_{3/2\,-1/2,1\,-1}\right]^2+3\left[C^{3/2\,-1/2}_{3/2\,-1/2,1\,0}\right]^2+\left[C^{3/2\,1/2}_{3/2\,-1/2,1\,1}\right]^2\right)}{6a}\right.\\
&\quad \left. + \frac{2\left[C^{5/2\,-3/2}_{3/2\,-3/2,1\,0}\right]^2\left(\left[C^{5/2\,-3/2}_{3/2\,-1/2,1\,-1}\right]^2+3\left[C^{5/2\,-1/2}_{3/2\,-1/2,1\,0}\right]^2+\left[C^{5/2\,1/2}_{3/2\,-1/2,1\,1}\right]^2\right)}{3(6a+5B)}\right\}\\
&= -\frac{d^2\langle r_C\rangle^2}{625R^8}\left(\frac{102}{6a}+\frac{108}{6a+5B}\right)
\end{aligned}
$$

into account the second order repulsion, producing the largest contribution to the splitting. The corresponding splitting Δ is given by

$$
\begin{aligned}
\Delta &= E\left(1^2\mathrm{A}'',\theta=\pi/2\right) - E\left(1^2\mathrm{A}',\theta=\pi/2\right)\\
&= 54\left(1+\frac{1}{2\mu_{(1,2)}}\right)^2\frac{\left(I^{(1,2)}_{10}\right)^2}{R\left(3I^{(1,2)}_{00}+2I^{(3,2)}_{00}\right)}\\
&\quad + \left(4+\frac{3}{\mu_{(1,2)}}+\frac{1}{\mu^2_{(1,2)}}\right)\frac{I^{(1,2)}_{20}}{R}\\
&\quad - \left(4+\frac{3}{\mu_{(1,4)}}+\frac{1}{\mu^2_{(1,4)}}\right)\frac{I^{(1,4)}_{20}}{R} > 0. \qquad \text{(A8)}
\end{aligned}
$$

4. Properties of the lowest adiabatic channel potentials

See Tables VI and VII for details.

[1] F. Lique, M. Jorfi, P. Honvault, P. Halvick, S. Y. Lin, H. Guo, D. Q. Xie, P. J. Dagdigian, J. Klos, and M. H. Alexander, J. Chem. Phys. **131**, 221104 (2009).
[2] D. C. Clary, Mol. Phys. **53**, 3 (1984).
[3] D. C. Clary and H.-J. Werner, Chem. Phys. Lett. **112**, 346 (1984).
[4] M. M. Graff and A. F. Wagner, J. Chem. Phys. **92**, 2423 (1990).
[5] J. Troe, Ber. Bunsenges. Phys. Chem. **99**, 341 (1995).
[6] M. Quack and J. Troe, Ber. Bunsenges. Phys. Chem. **78**, 240 (1974).
[7] E. E. Nikitin, J. Troe, and V. G. Ushakov, J. Chem. Phys. **102**, 4101 (1995).
[8] A. I. Maergoiz, E. E. Nikitin, J. Troe, and V. G. Ushakov, J. Chem. Phys. **105**, 6263 (1996).
[9] A. I. Maergoiz, E. E. Nikitin, J. Troe, and V. G. Ushakov, J. Chem. Phys. **105**, 6270 (1996).
[10] A. I. Maergoiz, E. E. Nikitin, J. Troe, and V. G. Ushakov, J. Chem. Phys. **105**, 6277 (1996).
[11] A. I. Maergoiz, E. E. Nikitin, J. Troe, and V. G. Ushakov, J. Chem. Phys. **108**, 5265 (1998).
[12] A. I. Maergoiz, E. E. Nikitin, J. Troe, and V. G. Ushakov, J. Chem. Phys. **108**, 9987 (1996).
[13] M. Auzinsh, E. I. Dashevskaya, I. Litvin, E. E. Nikitin, and J. Troe, J. Chem Phys. **139**, 084311 (2013).
[14] J. Troe and V. G. Ushakov, J. Chem. Phys. **128**, 204307 (2008).
[15] E. I. Dashevskaya, I. Litvin, E. E. Nikitin, I. Oref, and J. Troe, J. Phys. Chem. A **108**, 8703 (2004).
[16] E. E. Nikitin and J. Troe, J. Phys. Chem. A **114**, 9762 (2010).
[17] M. Auzinsh, E. I. Dashevskaya, I. Litvin, E. E. Nikitin, and J. Troe, J. Phys. Chem. A **115**, 5027 (2011).
[18] E. I. Dashevskaya, I. Litvin, E. E. Nikitin, and J. Troe, Mol. Phys. **108**, 873 (2010).
[19] M. Quack and J. Troe, Ber. Bunsenges. Phys, Chem. **79**, 170 (1975).
[20] M. Quack and J. Troe, in *Encyclopedia of Computational Chemistry*, edited by P. von Ragué Schleyer, N. Allinger, T. Clark, J. Gasteiger, P. A. Kollmann, and H. F. Schaefer (Wiley, New York, 1998), p. 2708.
[21] E. J. Rackham, T. Gonzalez-Lezana, and D. E. Manolopoulos, J. Chem. Phys. **119**, 12895 (1994).
[22] M. Quack and J. Troe, Ber. Bunsenges. Phys. Chem. **79**, 469 (1975).
[23] J. Troe, V. G. Ushakov, and A. A. Viggiano, Z. Phys. Chem. **219**, 715 (2005).
[24] D. C. Clary and J. P. Henshaw, Faraday Discuss. Chem. Soc. **84**, 333 (1984).
[25] M. Ramillon and R. McCarroll, J. Chem. Phys. **101**, 8697 (1994).
[26] A. Zanchet, B. Bussery-Honvault, and P. Honvault, J. Phys. Chem. A **110**, 12017 (2006).
[27] A. Zanchet, P. Halvick, J.-C. Rayez, B. Bussery-Honvault, and P. Honvault, J. Chem. Phys. **126**, 184308 (2007).
[28] B. Bussery-Honvault, F. Dayou, and A. Zanchet, J. Chem. Phys. **129**, 234302 (2008).
[29] A. Zanchet, B. Bussery-Honvault, M. Jorfi, and P. Honvault, Phys. Chem. Chem. Phys. **11**, 6182 (2009).
[30] A. Zanchet, T. Gonzalez-Lezana, O. Roncero, M. Jorfi, P. Honvault, and M. Hankel, J. Chem. Phys. **136**, 164309 (2012).
[31] T. Rajagopala Rao, S. Goswami, S. Mahapatra, B. Bussery-Honvault, and P. Honvault, J. Chem. Phys. **138**, 094318 (2013).
[32] A. I. Maergoiz, E. E. Nikitin, J. Troe, and V. G. Ushakov, in *Theory of Chemical Reaction Dynamics*, edited by A. Lagana and G. Lendvay (Kluwer Academic, Dordrecht, 2004), p. 21.

[33]C. Xu, D. Xie, D. H. Zhang, S. Y. Lin, and H. Guo, J. Chem. Phys. **122**, 244305 (2005).
[34]M. Jorfi, P. Honvault, P. Bargueno, T. Gonzalez-Lezana, P. Larregaray, L. Bonnet, and P. Halvick, J. Chem. Phys. **130**, 184301 (2009).
[35]G. Quemener, H. Balakrishnan, and B. K. Kendrick, Phys. Rev. A **79**, 022703 (2009).
[36]J. Ma, S. Y. Lin, H. Guo, Z. Sun, D. H. Zhang, and D. Xie, J. Chem. Phys. **133**, 054302 (2010).
[37]A. Li, D. Xie, R. Dawes, A. W. Jasper, J. Ma, and H. Guo, J. Chem. Phys. **133**, 144306 (2010).
[38]T. Stoecklin, B. Bussery-Honvault, P. Honvault, and F. Dayou, Comp. Theor. Chem. **990**, 39 (2012).
[39]A. J. C. Varandas, J. Chem. Phys. **138**, 134117 (2013).
[40]O. Rosmus, P. Palmieri, and R. Schinke, J. Chem. Phys. **117**, 4871 (2002).
[41]R. Dawes, P. Lolur, J. Ma, and H. Guo, J. Chem. Phys. **135**, 081102 (2011).
[42]M. Lepers, B. Bussery-Honvault, and O. Dulieu, J. Chem. Phys. **137**, 234305 (2012).
[43]M. Jorfi and P. Honvault, J. Chem. Phys. **133**, 144315 (2010).
[44]N. Bulut, O. Roncero, M. Jorfi, and P. Honvault, J. Chem. Phys. **135**, 104307 (2011).
[45]C. Xie, A. Li, D. Xie, and H. Guo, J. Chem. Phys. **135**, 164312 (2011).
[46]J. Daranlot, M. Jorfi, C. Xie, A. Bergeat, M. Costes, P. Caubet, D. Xie, H. Guo, P. Honvault, and K. M. Hickson, Science **334**, 1538 (2011).
[47]B. Bussery-Honvault and F. Dayou, J. Phys. Chem. A **113**, 14961 (2009).
[48]R. N. Zare, *Angular Momentum: Understanding Spatial Aspects in Chemistry and Physics*, Baker Lecture Series (Wiley, New York, 1988).
[49]L. D. Landau and E. M. Lifshitz, *Quantum Mechanics Non-Relativistic Theory*, 3rd ed. (Butterworth-Heinemann, New York, 1981).
[50]A. A. Radzig and B. M. Smirnov, *Reference Data on Atoms, Molecules, and Ions*, Springer Series in Chemical Physics (Springer-Verlag, Berlin/New York, 1985), Vol. 31.
[51]M.-L. Dubernet, D. Flower, and J. M. Hutson, J. Chem. Phys. **94**, 7602 (1991).
[52]W. R. Gentry and C. F. Giese, J. Chem. Phys. **67**, 2355 (1977).
[53]P. E. Cade and W. M. Huo, J. Chem. Phys. **47**, 614 (1967).
[54]K. I. Peterson, G. T. Fraser, and W. Klemperer, Can. J. Phys. **62**, 1502 (1984).
[55]D. Spelsberg, J. Chem. Phys. **111**, 9625 (1999).
[56]E. Nikitin and S. Ya. Umanskii, *Theory of Slow Atomic Collisions*, Springer Series in Chemical Physics (Springer-Verlag, Berlin/New York, 1984), Vol. 30.
[57]S. Ya. Umanskii and E. E. Nikitin, Theoret. Chim. Acta **13**, 91 (1969).
[58]A. J. C. Varandas and A. I. Voronin, Chem. Phys. **194**, 91 (1995).
[59]E. E. Nikitin, Ch. Ottinger, and D. V. Shalashilin, Z. Phys. D **36**, 257 (1996).
[60]See supplementary material at http://dx.doi.org/10.1063/1.4889996 for asymptotic contributions to the PESs calculated without SO-coupling.